5-2021

Testing and Performance Analysis of a New Wireless Sensors Network (WSN) System for Hurricane Monitoring

Jianing Wang

Testing and Performance Analysis of a New Wireless Sensors Network (WSN) System for Hurricane Monitoring

by

Jianing Wang

A thesis submitted to the College of Engineering and Science of
Florida Institute of Technology
in partial fulfillment of the requirements
for the degree of

Master of Science
in
Aerospace Engineering

Melbourne, Florida
May, 2021

We the undersigned committee hereby approve the attached thesis,
"Testing and Performance Analysis of a New Wireless Sensors Network (WSN) System for Hurricane Monitoring"
by
Jianing Wang

Chelakara S. Subramanian, Ph.D
Professor
Aerospace, Physics and Space Sciences
Major Advisor

Jean-Paul Pinelli, Ph.D
Professor
Mechanical and Civil Engineering
Committee Member

Steven Lazarus, Ph.D
Professor
Ocean Engineering and Marine Sciences
Committee Member

David Fleming, Ph.D
Associate Professor and Department Head
Aerospace, Physics and Space Sciences

Abstract

Title: Testing and Performance Analysis of a New Wireless Sensors Network (WSN) System for Hurricane Monitoring

Author: Jianing Wang

Major Advisor: Chelakara Subramanian, Ph.D.

Researchers at the Florida Institute of Technology (FIT) have developed the wireless sensor network system for the field measurement of hurricane wind and pressure on residential structures. A new version of the system is developed using the latest state-of-the-art technologies which performance is tested during the passing of hurricane Isaias (2020) and the Wall of Wind (WOW) at Florida International University (FIU). The old version system sensors were applied during hurricane Dorian (2019). For the three events, 25 pressure sensors and one anemometer were placed on the roof of a single-story house. Hurricane Dorian data was collected for 72 hours in total from September 2, 2019, and Hurricane Isaias for 78 hours from August 1, 2020. The WOW tests were performed on September 3, 4, and 8, 2020. The data of pressure, wind speed, and wind direction were continually collected. The project goal is to establish the accuracy of the new generation of WSN system and analyze the pressure and wind fluctuation characteristics of the hurricanes and WOW test. Various statistical analysis, including spectral analysis, is performed to study the influence of the corner vortex on the pressure. The result estimates the acceleration effect, separation effect acting on different areas of the roof. The power spectrum density (PSD) plots, one of the outcomes of spectral analysis, corresponds to the strength of the fluctuation on different frequencies of the flow.

The WSN system measures air pressure, humidity, temperature, wind speed, and wind direction, where humidity is added to the system for the first time. This paper introduces the hardware comparison between two generations of WSN systems in terms of pressure resolution. The dimensions are also involved in the comparison for pressure sensor case,

circuit board, and coordinator. The pressure sensor case WSN system performance analysis shows the comparison of pressure measurement by two generations of the WSN system. The resolution is a 0.1 mbar for the pressure measurement of the new system, which is around 1/25 of the old system. For other measurable values, they all get significant improvements which resolution will be explained.

The agreement of spectral analysis results for corner vortices and flow separation is less pronounced between hurricanes and WOW test, but the trends are similar. The wind properties constantly change, leading to the impure PSD plots. Corner vortices at the leeward roof cause the pressure fluctuation along the windward roof edge and lead to the large PSD on the frequency domain. The acceleration effect acting on the roof leeward eliminates pressure fluctuation, but the separation acting on the leeward area increases the pressure fluctuation.

Table of Contents

List of Figures

List of Tables

Acknowledgement

I would like to thank my thesis advisor, Dr. Chelakara Subramanian. Also grateful to Dr.Jean- Paul Penelli and Dr. Steven Lazarus who helped me with the new WSN design and testing and gave me many valuable suggestions on the Hurricane measurement. Mr. Jialin, MS-Mechanical Engineering graduate, helped to develop the entire WSN software system. Mr. Jian Zhang and Ms. Soundarya Sridhar helped me with the data processing of the WOW and hurricane data. This project was funded by the NIST program 70NANB19H088- Wireless Sensor Network (WSN) System and LIDAR Experiments for the Characterization of Strong Wind Loads on Non-Structural components and Near-Surface Wind Profiles starting in 2019.

Last, my thanks would go to my family for their loving considerations and great confidence in me all through years. I also owe my sincere gratitude and love to my girlfriend Yingnan Zhai for her encouragement and moral support.

Chapter 1
Introduction

The formation of tropical storms and hurricane is a fascinating phenomenon involving fluid dynamics and thermodynamic interactions. A low-pressure system moving over the warm ocean water forms the beginning of a hurricane. The cooler atmosphere from higher altitudes absorbs the heat from the warm seawater and starts moving westward by summer-monsoon circulations. In the meantime, the thunderstorms make the system become organized and warmer. When the storm is still located at the north of the equator, the Coriolis effect rotates the storms counterclockwise that increase the wind speed around the center and creates the center of the storm (Holland, 1980; Ramage, 1959). The hurricanes are more likely to form out of the 5-degree latitude of the equator. The low vertical wind shear in the upper atmosphere varies the speed with height and limits the accent of the parcels. The wind speed increases around the storm center. The *tropical depression* is associated with wind speeds up to 38 miles per hour, the *tropical storm* wind speeds exceed more than 39 miles per hour, and finally, the *hurricane* wind speed exceeds 74 miles per hour (Ramage, 1959).

Hurricanes have affected Florida for many decades and caused significant damage. Since 1980, the cumulative impact from the hurricane has risen to $1.86 trillion in U.S., with an alarming number of human lives. Although we are trying to study hurricanes , it is a constant learning from more and more hurricanes in order to eventually develop a robust prediction tool to prevent damage of the properties due to the storm surge, flooding and strong wind. The strong wind speed may overturn the tree to the building. More significantly, the wind flow over the roof generates the huge suction force that rips shingles off the roof, even raise the entire roof (Coch, 2020). The wind speed for a hurricane is clarified by the Saffir-Simpson scale, which starts at the category one hurricane with at least 74 miles per hour and ends with the minimum wind speed of 157 miles per hour shown in Table 1 (Schott, 2019).

Table 1 The Saffir-Simpson Hurricane Scale Updated on January 2, 2019

Category	Hourly Avg. Sustained Winds (miles per hour)
Tropical Storm	39-73
Cat. 1	74-95
Cat. 2	96-110
Cat. 3	111-130
Cat. 4	131-156
Cat. 5	157 or higher

Until 2018, the old wireless sensor network (WSN) systems were deployed in hurricanes due to its major advantages, viz., wireless and weatherproof qualities. The WSN system contains all sensors to measure data and software to gather data from the sensors. Taking advantage of the previous system, in 2019, the building of the latest WSN system began. This system made significant improvements in accuracy and quantities of measurement. In addition, the software system readily synchronizes the data transfer on Cloud storage services such as the DesignSafe. During the system development, several glitches of hardware and software were solved.

The performance of the new WSN was tested in two hurricanes which impacted the Florida east coast between Fall 2019 and October 2020. Calibration of the WSN system was also performed in the Florida International University's (FIU), Wall of Wind (WOW) experimental facilities.

Hurricane Dorian, a category-5 hurricane, moved up the east coast of Florida with the eye keeping 110 miles away from landfall (Alfonso & Hayes, 2019). To train in the deployment process and strategies, as well to compare the performance with the future new system, between September 2 to 5, 2019, the previous sensor system, including 13 pressure sensors, one reference pressure sensor, and one anemometer, were deployed on the roof of a house (Jack's house) located at Satellite Beach. Around this site, the tropical-storm-force winds were recorded on September 3, 2019 (Mazzei & Bogel-Burroughs, 2019).

Unfortunately, the anemometer failed to record, so only the pressure measurements were recorded by the WSN system.

Hurricane Isaias was a category-1 hurricane that followed a similar path on Ang. 1st, 2020 as Dorian's, but with less strength. At that time, the prototype version of the two new-generation hurricane pressure sensors, a reference pressure and an anemometer, were installed together with the sixteen previous generation pressure sensors and an anemometer located on the roof of Jack's house. The layout of the sensors for this deployment is shown in Chapter 2. To monitor the surrounding wind field, a Lidar was also co-located within 300 yards distance on the beach.

On September 3, 2020, the completed new generation of WSN sensors was tested in the FIU WOW facilities. The system included 25 pressure sensors, a reference pressure sensor, and an anemometer. The WOW can simulate winds up to a category-4 hurricane on a full-scale (11'x10'x10') single-story building. (Aly, Bitsuamlak, & Chowdhury, 2011).

Table 2 Testing Information for Hurricanes Dorian, Isaias, and WOW Testing

Hurricane or WOW Testing	WSN System Used	Test Site	Peak Wind Direction
Dorian (Cat. 5)	Previous Only	Jack's House, Satellite Beach	Northwesterly
Isaias (Cat. 1)	Previous and Latest	Jack's House, Satellite Harbour Beach	Northerly
WOW Testing	Latest Only	WOW facility, FIU	360 degrees

Data Processing and Analysis

The main objective of the hurricane project was to measure and analyze the fluctuation of the pressure on the structural components of the residential home. Since the pressure varies significantly during hurricanes, first, the trendline of pressure was plotted using 5-mins moving averaging. Second, an obvious pressure decrement occurred where the hurricane is approaching the location of deployment. The range of the pressure variation was determined. Secondly, the root mean square of pressure (RMS) during periods of decreasing average pressure was calculated. RMS value quantifies the pressure fluctuations. Then, spectral analysis, using Discrete Fourier Transform (DFT), was performed to determine the frequency contents of pressure fluctuations.

The main objective of WOW testing was to compare the WSN system against the Scanivalve pressure measurements for the full-scale measurements. The differential pressure is obtained by subtracting pressure sensor readings from the reference pressure sensor reading, which is located inside the test house. That is compared with the FIU Scanivalve differential pressure measurement at the corresponding locations. The root means squared distribution of differential pressure was compared with the hurricane measurement. The Spectral analysis results were also similarly compared.

Overview of WSN System

The WSN system is built for monitoring the wind pressure and speed on the residential structures during extreme weather, such as hurricanes and tropical storms. The overall architecture of the sensor network system is similar to the previous system, containing three functional subsystems, shown in Figure 1. The first subsystem is responsible for measuring and data transferring, including remote sensors such as pressure sensors and anemometers. The second subsystem is the network communication from the laptop and base unit to the central server, such as Cloud storage through the public Internet. Finally, the third subsystem is a central server, which stores the data and processes the raw digital data to physical data (Lapillia, Chandiramanib, Kostanicc, Pinelli, & Subramaniane, 2010). In a nutshell, in the WSN system, pressure sensors and anemometer sample data are sent by a dedicated local wireless network to the base and laptop, which collects the data and sends them to the cloud storage via the public Wi-Fi network (Figure 1).

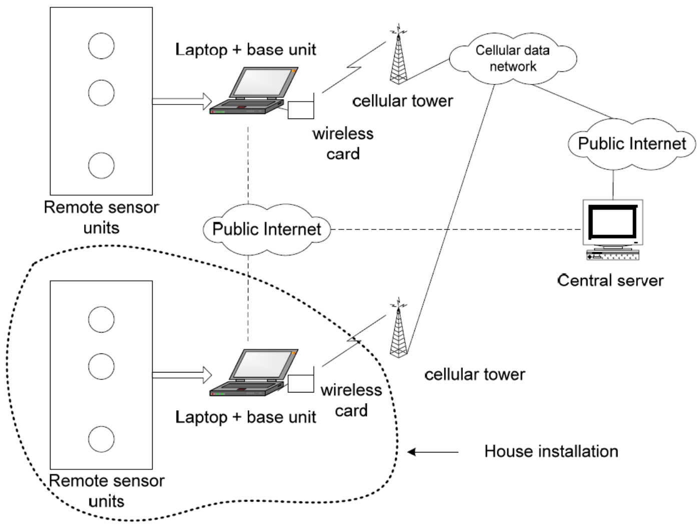

Figure 1 The Diagram of WSN System

With the same architecture of the old WSN system, the new WSN system upgrades the accuracy of pressure, humidity, temperature, wind speed, and direction. (See Appendix A: WOW Sensors Test Layout). The redesigned software synchronizes the data file to the Cloud storage during measurement. In addition, Figure 2 and Figure 3 indicate the major modification in the shape of the base unit and pressure sensor. The base unit is miniaturized as a USB drive from a box of the old system. The pressure sensor becomes smaller than that of the old system. The physical deployment, modified to make the sensors easier to install, is critical for broadening the deploy type of surface. The circuit board of the new system (Figure 4) contains a high-performance main control unit (MCU), ATSAM21, where the analog to digital converter (ADC) is 14 bits of resolution. With the oversampling method, the resolution of the readings increases to 16 bits. The resolution of measurements for air pressure, humidity, temperature, wind speed, and wind direction are 0.1 mbar, 0.03%RH, $0.05°C$, 0.05m/s and 0.005 degree, respectively. The sensors' names and model numbers are listed in Table 3. Also, the circuit board adds the expansion port, which contains two analog and two digital ports for future requirements of hurricane measurement. To date, the wind speed and direction, humidity, and GPS location are measured through the expansion ports.

Table 3 Sensor Model Number List

Sensor Unit	Pressure	Temperature	Humidity	Anemometer
Model Number	MP3H6115AC6T1	MCP9700T	HIH-5030	05103V

A complete system contains up to 30 pressure sensors, one reference pressure sensor, and one anemometer. Pressure sensors and reference pressure sensors measure absolute pressure acting on the roof and inside a chamber at rest (stagnation pressure). Anemometers measure wind speed and direction. The Xbee modules generate a Zigbee network coexisting with 2.4 GHz Wi-Fi. The network carries the communication between all nodes (sensors) and a coordinator (base unit). Each sensor is equipped with an Xbee module to transfer the data packages to the coordinator. Cyclic Redundancy Checker (CRC) in the software checks the data's completeness and decides whether it will be accepted. Table 4 illustrates other essential features of the new and old system. The new system case has a smaller size than the old system. The only deployment method (wing nuts) of the old system limits the measurement condition. The wing nut bolts are installed in the roof and walls and leave permanently. It takes a long time to finish that job and is rejected by the house owner. Since 2019, researchers in FIT were looking for a safe and fast method to attach the sensors to the surface of the house safely which are able to be move easily. Finally, after been repeatedly tested in the lab, the combination of the Velcro pads and E-poxy was settled. Three Velcro pads of the hairy side attach to the bottom of the sensor using E-poxy, and their pads of the hook side place on the rough surface such as shingles of the roof (Figure 6). The usage of the E-Poxy is necessary to fill the gap between the pads with the surface attached (Figure 7). The same method was also tested during WOW to find the maximum speed for securing the sensor. It tested out that the maximum wind speed was 90 mph before the Velcro came off the wall. Figure 8 shows the sensor remains which were blown down from the house. The Xbee module transfers data to the base unit which the communication range determined the maximum distance that a sensor can locate from the base. Both two versions of Xbee equipped on generations of WSN system give 3200m at outdoor and 90 m at indoor condition. But during the field test for the new system, they decrease to 179m and 35m, which were tested in Murano Dr, and

Olin Engineering Complex, FIT, Melbourn, FL. Both systems equip the routers which transfer the data packages from the sensors out of the range to the base unit. For the new system, each router can transfer data from up to 20 sensors. Instead of 110V wall power, the solar charging system enables the charging function during the measurement, hence keeps the system work for a long duration.

Table 4 Important Features Comparison of the New vs. Old System

System	Case Diameter	Case Heigh	Deployment Method	Solar Charging	Xbee range
New	240 mm	53 mm	Velcro or Screws	Yes	3200 m (outdoor) 90 m (indoor)
Old	350 mm	45 mm	Wing nuts	No	3200 m (outdoor) 90 m (indoor)

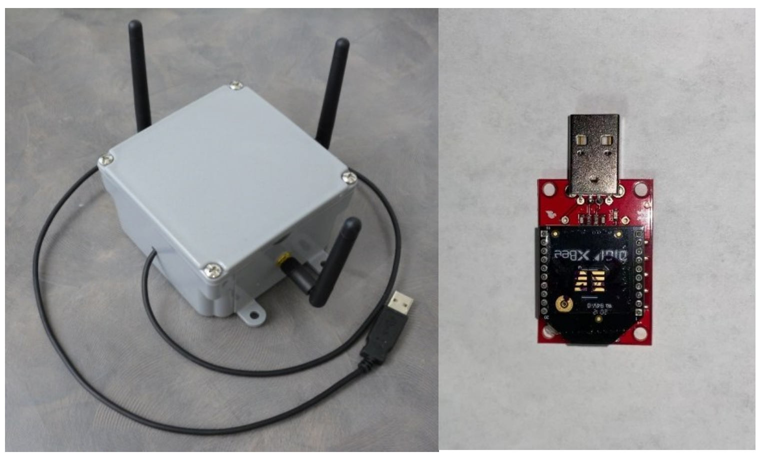

Figure 2 Comparison of a Base Unit of Old (Left) and New (Right) System

Figure 3 Comparison of a Pressure Sensor of Old (left) and New (Right) System

Figure 4 Circuit Boards Comparison of Old (Left) vs. New (Right) System

To meet the functional requirement of the WSN system, the WSN graphical user interface (GUI), powered by Windows Presentation Foundation (WPF) of .NET Framework, collects data from the base unit through the serial port and saving data on the local and cloud storage (DesignSafe). The GUI also supports the real-time data plotting function where all sensors detected in the Zigbee network are shown in the plot on the GUI window. The GUI also equips CRC, the last checker for the data completeness before it saves data in the computer as Comma-Separated Values (CSV) data file (Sun & Wang, 2020). Despite saving locally and cloudly, the GUI of the new system also uploads to the database server provided by FIT to generate the real-time plots for public broadcasting without any interference to the WSN system.

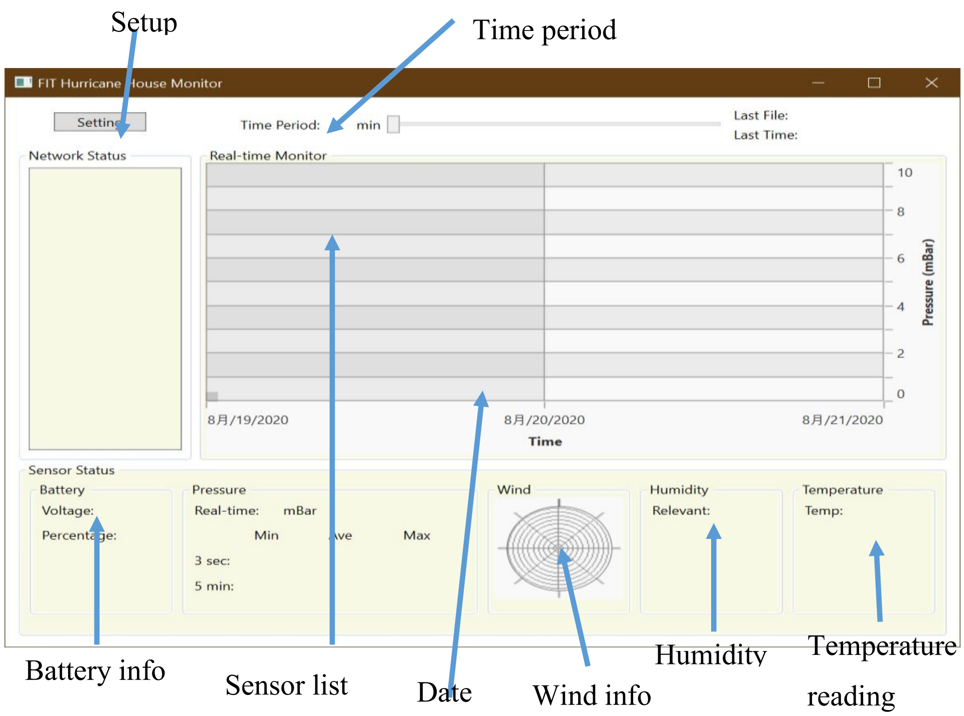

Figure 5 Hurricane House Monitor Program Display Panel

Figure 6 Layout of the Velcro (Top) and Epoxy (Mid) Applied on a Surface (Bottom)

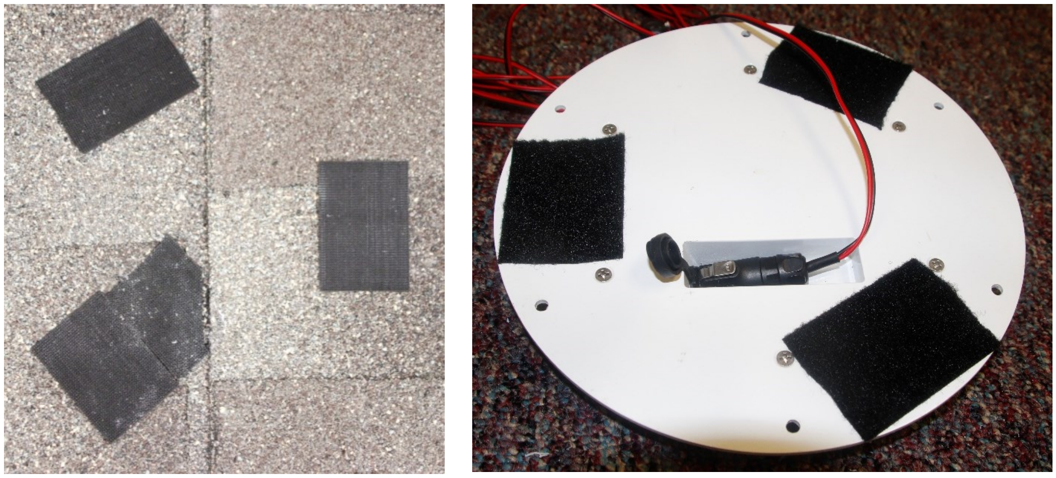

Figure 7 Velcro Pads Attached on a Sensor and the Shingles

Figure 8 The Sensor Remains after Being Blown Down from the House at 90 mph

Physical Aspects of Hurricane Dorian

The entire track path was published by National Hurricane Center (Figure 9). Hurricane began as a large tropical wave at the west coast of Africa on August 19, 2019, and crossed the tropical Atlantic, where the wave lost most of the associated thunderstorm activity. The cyclonic circulation developed along 40° and moved west, developing into a tropical depression at about 700 nautical miles (805 miles) away from east-southeast of Barbados in the Windward Islands at 0600 UTC August 24 (Avila, Stewart, Berg, & Hagen, 2019). The tropical depression contented the better organization and further developed as Tropical Strom Dorian at 1800 UTC August 24, which the influential curved convective band wrapped around the eye. After 24 hours, Dorian had peak winds of 45 knots and was not organized well due to the dry air encounter when it reached the Windward Islands. Dorian moved across the Windward Islands, where it caused the landfall with a strong cyclone and a 45-knot wind force. The high mountains on the islands added much disturbance to the cyclone. The center then re-formatted to the north. Dorian continually moved northwest and formed the eyewall while the pressure dropped (Avila, Stewart, Berg, & Hagen, 2019). Moving away from the Windward Islands, Dorian crossed the western tip of St. Thomas in the U.S. Virgin Islands at 1800 UTC August 27 and propelled into the Atlantic. The pressure dropping between upper-level low over the Straits of Florida and the Atlantic subtropical ridge pushed the Dorian west-northwest. The very warm sea water made Dorian a category 3 hurricane on the Saffir-Simpson Hurricane Wind Scale at 1800 UTC August 30. (Avila, Stewart, Berg, & Hagen, 2019) At the end of this day, the estimated wind speed of surface increased to 115 knots (Figure 11). A category 5 hurricane developed with the eye of 12 nautical miles in diameter and the surface speed of 160 knots (Figure 11). The central pressure decreased to 910 mbar on September 1, 2020. Moving slowly west, Dorian impacted Great Abaco for 3 days and speeded up westward to Grand Bahama Island and Florida. Dorian turning north-northwest at 5-10 knots east of Florida from September 3-5, 110 miles away from landfall (Alfonso & Hayes, 2019; Avila, Stewart, Berg, & Hagen, 2019). The high shear of the air and cooler water weakened the hurricane, however Dorian strengthened back when it reached Georgia and South Carolina on September 5. Then the hurricane speeded up northward to North Caroline but weakened as a category 1, then became a post-tropical cyclone on September 7, 2019 before it reached Nova Scotia and Canada. In total, Dorian caused 84 fatalities and 245 missing. $4.68 billion lost during the hurricane recorded among the Lesser Antilles, Bahamas, United States, and Canada (Mazzei & Bogel-Burroughs, 2019; Avila, Stewart, Berg, & Hagen, 2019). The official track was published by National Hurricane Center (Figure 9)

Since the center of Dorian stated offshore the eastern coast of Florida, the highest measured surface wind speed in the State was 60 knots (31m/s) at a tropical-storm force at around 0604 UTC September 4 (Avila, Stewart, Berg, & Hagen, 2019). At 0935 UTC, Dorian reached the closest distance from Cocoa Beach, where the measured inland wind speed was 46 knots (23.66m/s) and pressure was 998.1 mbar (Avila, Stewart, Berg, & Hagen, 2019; Mazzei & Bogel-Burroughs, 2019). When Dorian moved fast along the Florida eastern coasts, the cumulation of rainfall was less than 2.99 inches (Figure 10).

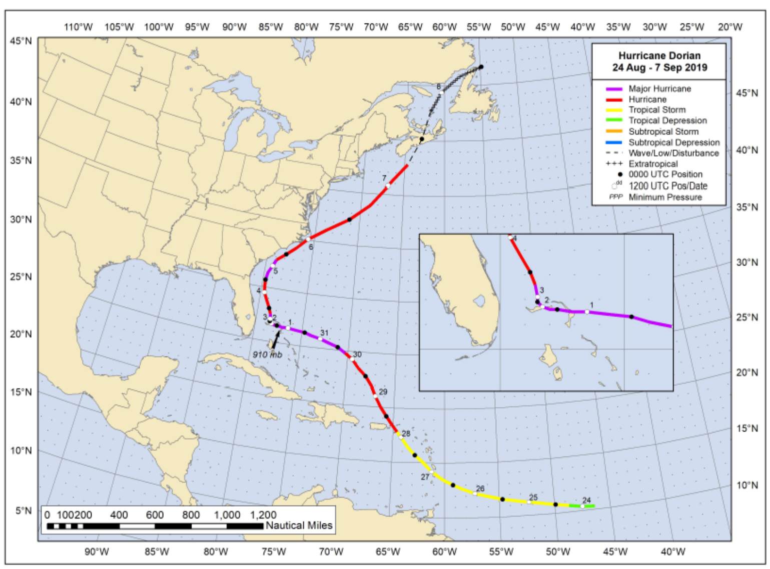

Figure 9 The Official Track of Hurrican Dorian from August 24, 2019 to September 8, 2019 by National Hurricane Center

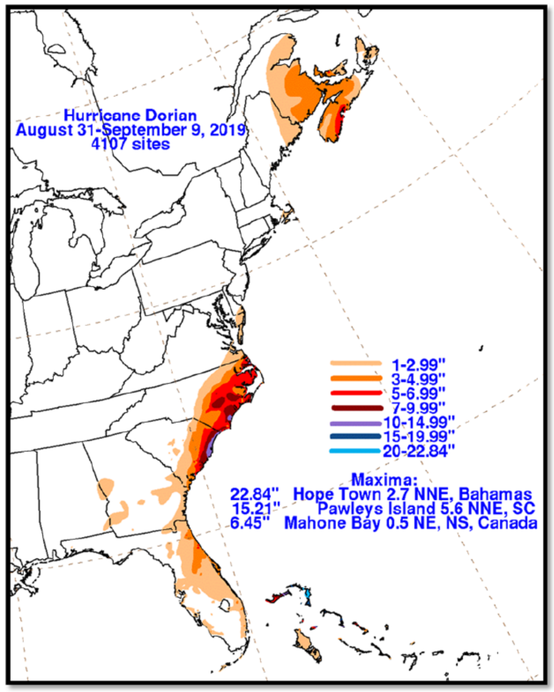

Figure 10 Hurricane Dorian Rainfall (inches) from August 31 to September 9, 2019, by NOAA Weather Prediction Center

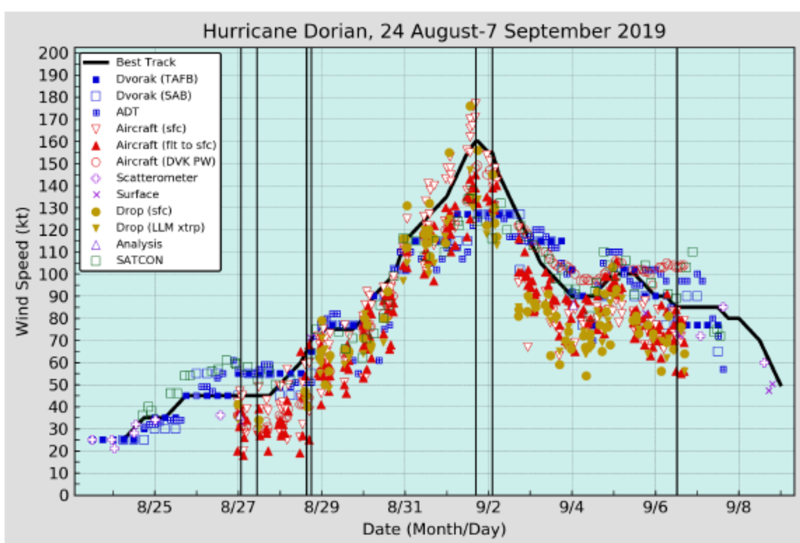

Figure 11 Wind Observation of Maximum Sustained Wind Speed for Dorian August 24 to September 7, 2019

Physical Aspects of Hurricane Isaias

National Hurricane Center did not publish the official report but based on the public advisories from July 28 to August 5. Isaias began as a tropical wave west of Africa on July 23, 2020 and crawled west to northwest crossing the Atlantic (Beven, 2020). At 15:00 UTC July 28, 2020, the system was organized as an area of low pressure and continue to move westward to Dominica. An official named tropical storm Isaias formed south of Dominica on 0300 UTC July 29 from a well-developed tropical cyclone system that had already obtained gale-force wind (Pasch, Tropical Storm Isaias Discussion Number 7, 2020). Isaias caused landfall on the south coast of Dominica and was strengthened, which the wind speed raised to 52 knots. The intensity of Isaias kept increasing due to a new low area formed north of Isaias. It was officially classified as Category 1 hurricane with a wind speed of 70 knots and 990 mbar of minimum central pressure at 0300 UTC July 31, 2020. Isaias limited the intensity due to the dry air and southwesterly shear, but it strengthened back within a day with a clear eye where the minimum pressure reached 987 mbar (Pasch, Hurricane Isaias Intermediate Advisory Number 15, 2020). The wind speed of the hurricane was 74 knots when Isaias made landfall on Northern Andros Island at 1500 UTC August 1, 2020 (Stewart, Hurricane Isaias Advisory Number 18, 2020). Isaias weakened below the level of Category 1 due to the lack of convection on its center, although it moved back over seawater before it arrived in South Florida (Stewart, Tropical Storm Isaias Discussion Number 19, 2020). When approaching Southeast Florida, the storm paralleled the east coast of Florida with around 60 knots of wind speed with the similar path of Dorian and was weakened to a tropical storm. It brought heavy winds and rainfall but damaged much less than expected due to the incomplete development. At 0300 UTC Aug 2020, Isaias center moved to the nearest location from Indian Harbour Beach, 46 nautical miles west of the Indian Harbour Beach (Bullentin, 2020). As reported, Isaias was continually moving northwest at 7.8 knots which central pressure is 995 mbar. A 51-mph wind gust was measured at the coast of Cape Canaveral and maintained above 49 mph of wind in 5 hours (Bullentin, 2020). During moving through the eastern coast of Florida, Isaias added about 5 inches of rainfall.

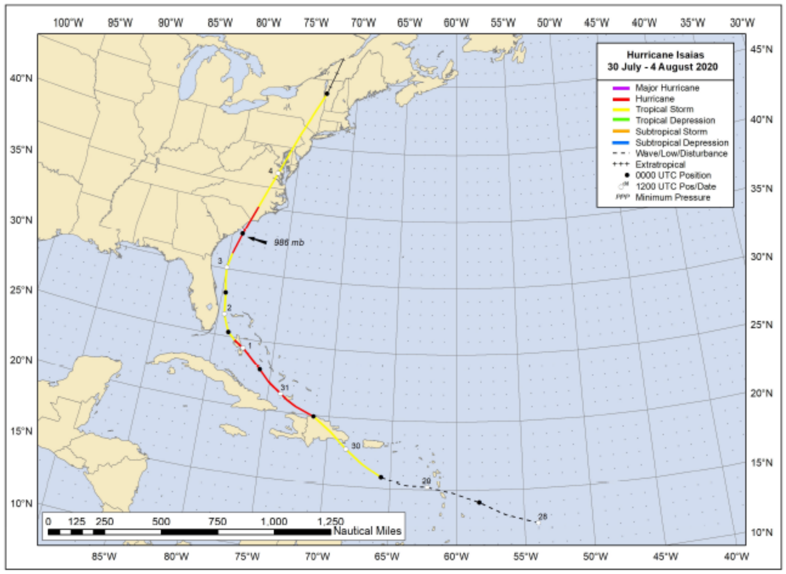

Figure 12 The Official Track of Hurrican Isaias from July 30 to August 4, 2020 by National Hurricane Center

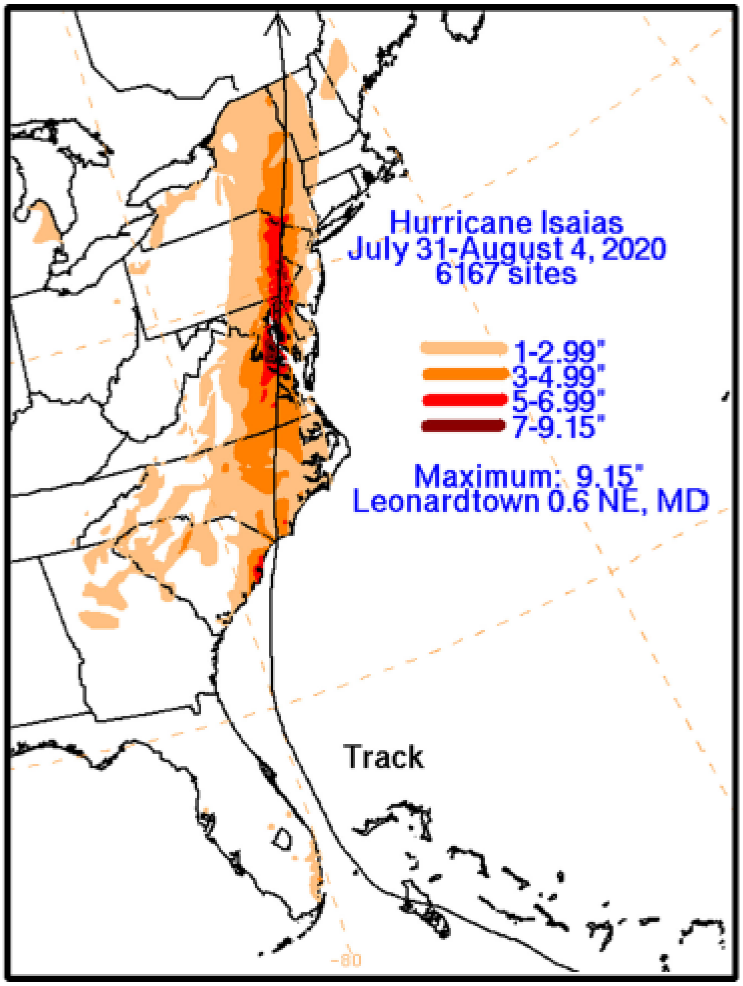

Figure 13 Hurricane Isaias Rainfall (inches) from July 30 to August 4, 2020, by NOAA Weather Prediction Center

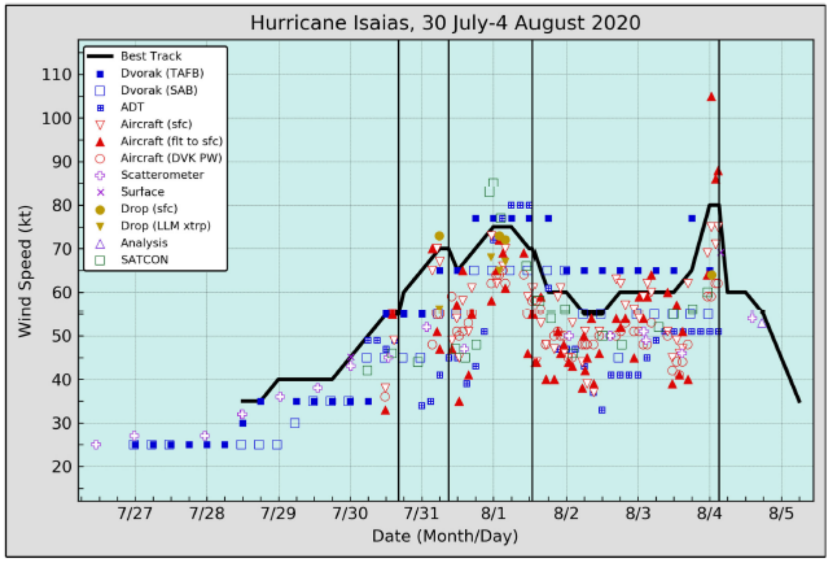

Figure 14 Wind Observation of Maximum Sustained Wind Speed for Isaias From July 30 to August 4, 2020

Wall of Wind

Wall of Wind (WOW) is a facility built by the International Hurricane Research Center (IHRC) of FIU (now an NSF NHERI facility) to simulate the interaction between simulated hurricanes and the buildings and improve the innovative hurricane mitigation development (Aly, Bitsuamlak, & Chowdhury, 2011).It generates the extreme condition as the real hurricane, such as rain and gust. WOW generates category 1 to 4 hurricanes and is large enough to contain a single-story, 11’x10’x10’, building model (Aly, Bitsuamlak, & Chowdhury, 2011). WOW is equipped with as many as 12 fans to generate wind fields to mimic hurricane winds (up to 157mph) and a water spray system (simulate a wind-driven rain conditions) to test the model under different weather conditions (Figure 15). WOW can simulate the two terrains of the building fetch (give the length), such as suburban (ASCE 7-16 Category B) and open terrain (ASCE 7-16 Category D), by changing the planks' pitch angles which determines the turbulence intensity profiles to suit suburban and open terrain (Aly, Bitsuamlak, & Chowdhury, 2011). The turntable (give the size) where the building models mounted can rotate 360^0 to achieve wind directions of the test (Figure 15). The turntable allows more tests at a limited time frame.

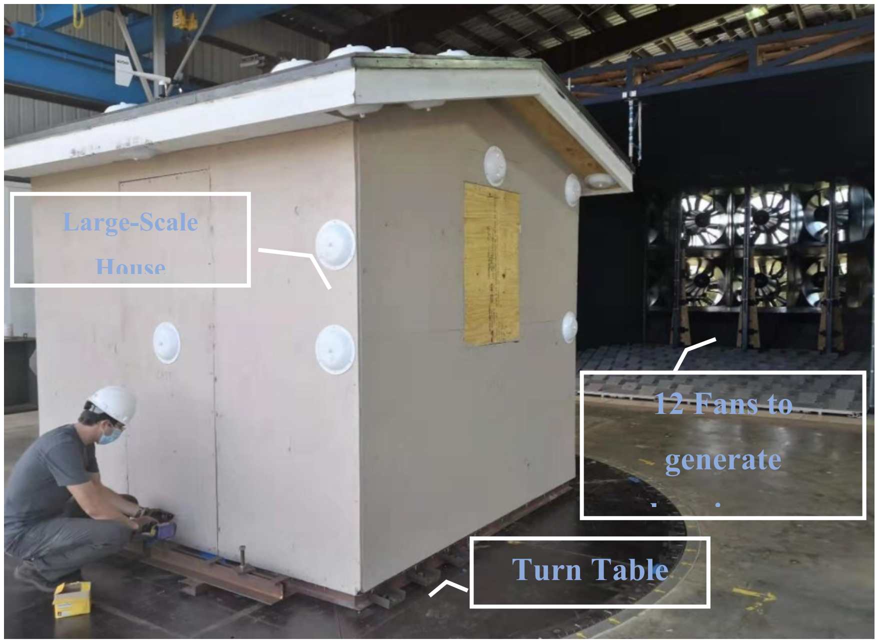

Figure 15 The Setup of The Model House, Including The House, Turntable, and The Fans

Chapter 2
Measurement of Hurricanes Dorian and Isaias and WOW

Dorian and Isaias Deployment and Measurement

The old WSN sensors system was deployed on Jack's house in Satellite Beach give 28.17N and 80.59W. During hurricane Dorian, 13 pressure sensors were installed on the roof and one reference pressure were located in a no wind area near Jack's house front porch, Figure (a). 14 pressure sensors were installed on the roof, and one reference pressure was located near Jack's house porch during hurricane Isaias, Figure(b). Between Dorian and Isaias, ten sensors are located at the same place on the roof, which can be used for comparison. The tracks of Dorian and Isaias are quite similar, and they moved north on the eastern coast of Florida. The north and east sides of the house were impacted during the hurricanes. Most of the sensors were placed on the eastern edge of the house, and two sensors were located on the north side of the roof. Pressure readings from each of the sensors for Dorian will be compared with corresponding readings for Isaias. For instance, Sensor 72 on the northeast corner roof and Sensor 80 of Dorian are compared with Sensor 74 and Sensor 80 of Isaias. All pressure sensor measures data at 10 samples per second.

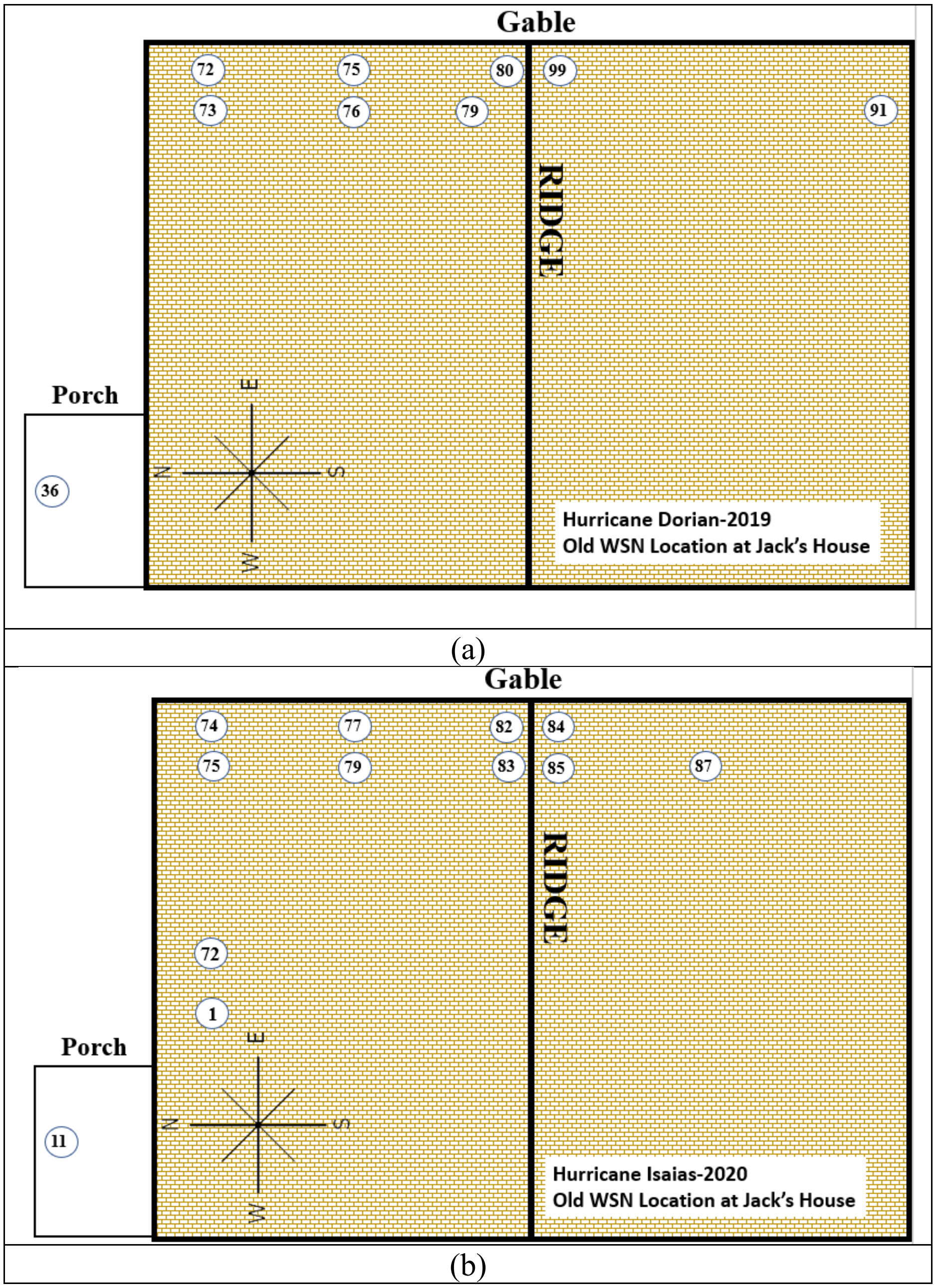

Figure 16 WSN Deployment Location on Jack's House During Dorian (a) and Isaias (b)

WOW Setup and Measurement and Sensor Layout

The WOW wind test is the experimental facility that simulates the hurricane wind give the range. A large-scale house (3.2 *3.4*2.9m) with the installed WSN sensors and FIU

Scanivalve sensors was located on a turntable to perform the test at the desired wind angle. Twelve fans generate wind speeds of up to 150 mph (category 4 hurricane) and produce a wind field with 4.3m high and 6.1m wide (Chowdhury, Moravej, & Zisis, 2019). 24 Sensors are fitted to the walls, roof, and soffit, as shown in the diagram. One reference sensor was set up inside the house to measure the pressure of the flow at rest (zero speed condition). The anemometer was located at the end of the roof ridge (Figure 18). Fourteen sensors were deployed on the roof (Figure 17), four sensors on the soffit (Figure 18 and 19), three on the north wall (Figure 18), three sensors on the east wall (Figure 19).

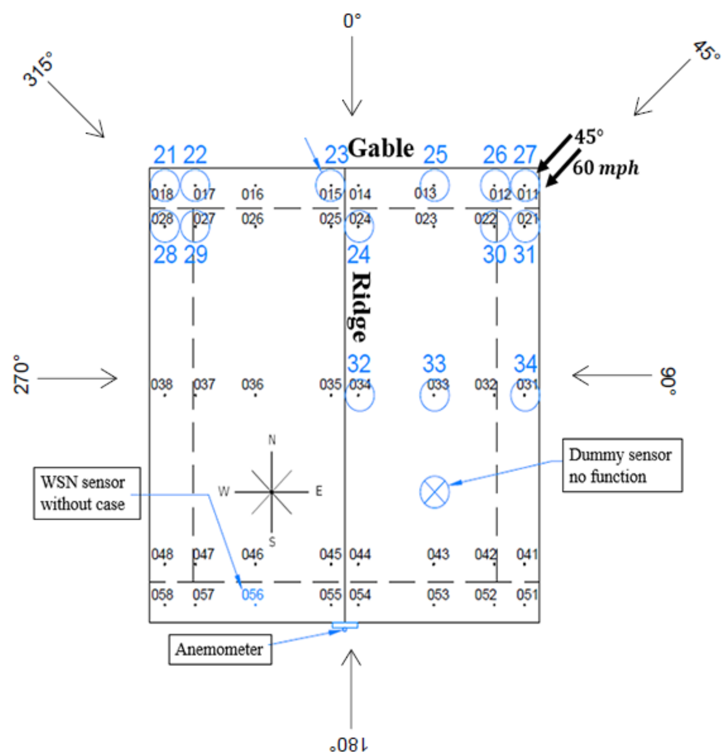

Figure 17 The layout of WSN Sensors and Scanivalve Taps on the Roof

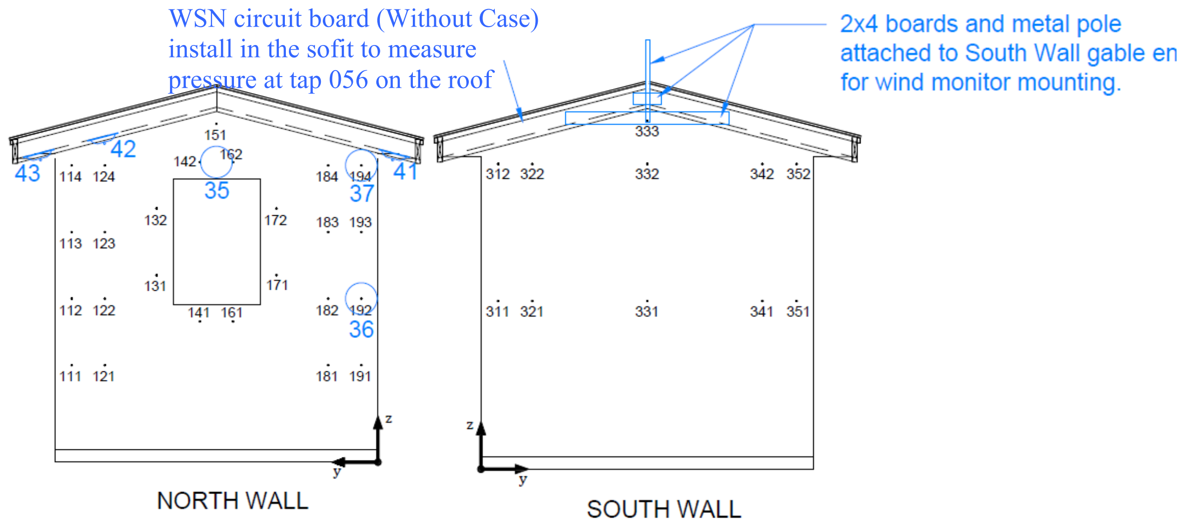

Figure 18 The Layout of WSN Sensors and Scanivalve Taps on North and South Walls

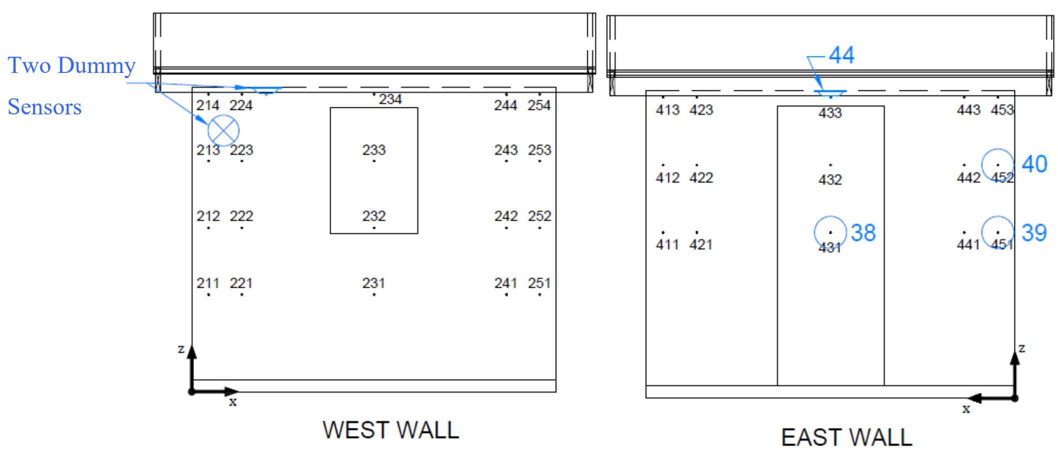

Figure 19 The Layout of WSN Sensors and Scanivalve Taps on West and East Walls

Each WSN sensor corresponds to a Scanivalve tap, shown in Table 5.Tests are performed for 30, 60, 90, 120, and 145 mph speeds at different angles of attack in 45° interval with respect to the house ridgeline,i.e., for 0°($northerly$), 45°, 90°, 135°, 180°, 225°, 270°, and 315°, under both rainy and dry conditions.

The height of a Scanivalve tap above the wall surface was within 2 mm (flush-mounted), whereas the size of a WSN sensor is 35 mm above the wall surface, which is the distance of the tube of the case to the attachment surface.

WSN WOW test started on 09/02/2020. Florida Institute of Technology deployed the WSN system on a 3.4m by 3.2m house model, mounted on a rotating table, in the FIU WOW. The primary objective was to calibrate the WSN system against the FIU’s Scanivalve sensors and test the Velcro's mounting technique. The strength of the Velcro test during the WOW. Three dummy sensors (only case) were installed on the house, including two dummy sensors mounted at the west side soffit and wall (Figure 19) and one mounted between tap location 033 with 043 (Figure 17) with the Velcro tape only. In addition, WSN sensor No.23 was mounted along the gable ridge with Velcro tape and safety wood screws and worked as a normal pressure sensor also a Velcro testing object.

The potential areas of the stagnation flow occur on the wall and the soffit which faces the flow, as the condition of sensors on the north wall and soffit at the angle of 0°. The laminar flow will occur on the windward roof. The turbulence potentially occurs on the leeward roof. Similarly, the effect of separation begins noticeable on the leeward roof, especially right after the ridgeline.

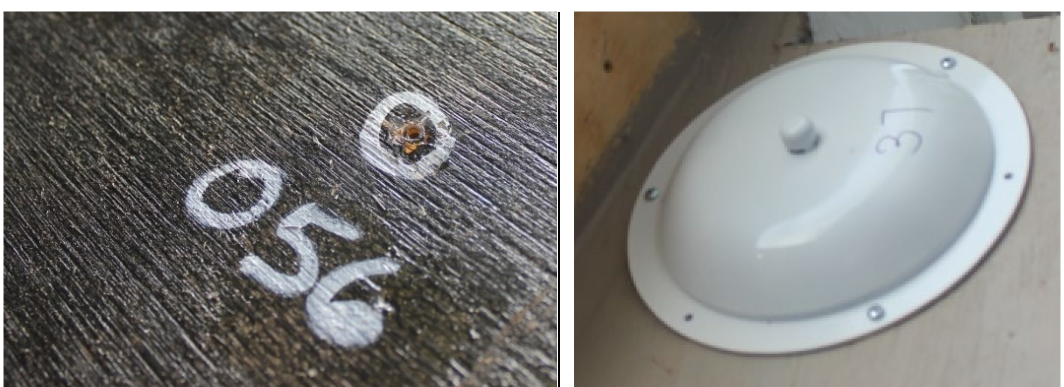

(a) (b)

Figure 20 Comparison Between a Scanivalve Tap (a) and a WSN Pressure Sensor (b)

Analysis of Hurricane measurements:

In this research, the author compares the pressure distribution on the house measured in the WOW and two Hurricanes, Dorian and Isaias. The spectral analysis is used to characterize the fluctuating pressure. For Hurricanes Dorian and Isaias, the pressure sensors were only located on the roof near edges and ridge, so the corresponding locations were chosen as the experimental comparison.

Chapter 3 Data Analysis Methods

Moving Average and Root Mean square

The hurricane winds produce both short-time and long-time fluctuations in properties. The moving average (MA) is commonly used with time-series data to smooth the short-time fluctuations and obtain the long-term trends. Whereas short-time fluctuations are used for calculating the fluctuating statistics like the root mean squared (RMS), Correlation coefficient, and Spectrum. Short-term and long-term trends are determined by the application and the window length. MA ensures the variations in the data are aligned with the variations in the mean (Kendall, 1979; Mann, 1945). In order to see the long-time trend properties, 5-min MA is recommended and applied on pressure trend plots during the hurricane. As for the spectral analysis, the raw data (no MA applied) is used because any MA may erase the potential fluctuation of pressure and decrement of PSD.

The Root mean square (RMS) pressure estimates are obtained from,

$$\boldsymbol{P_{rms}} = \sqrt{\frac{\mathbf{1}}{\boldsymbol{n}}(\boldsymbol{p}_{\mathbf{1}}^{\mathbf{2}}+..+\boldsymbol{p_n}^{\mathbf{2}})} \qquad \textbf{(1)}$$

, where Prms is the RMS pressure, and P1, P2,…and Pn are the instantaneous fluctuating pressures.

For the stationary period of pressure data, the time mean value of the pressure ($\bar{P}$) is regarded as constant, and the fluctuating pressure p is then determined from:

$$\mathbf{p} = \mathbf{P} - \bar{\mathbf{P}}, \qquad \textbf{(2)}$$

, where P is the instantaneous pressure.

Note that $\bar{P}(t, x) = \bar{P}(x)$, where x is the sample point of the data.

Mann-Kendall Tester

For the WOW tests, the test was performed for fixed angle, and fixed wind speed, so the data for each test setting is stationary. As for the natural hurricanes, Dorian and Isaias, the stationary window is determined by the reverse arrangements test (RAT), a statistical method to measure the significance of mean trends. The RAT determines the length of a stationary window after the data point is analyzed. Mann-Kendall tester (MKT) packages the RAT to a time series of data with a level of confidence (Fatichi, 2009). The MKT's output is a Boolean value,1 or 0, to reject a null hypothesis that a trend absence in the time series,$Rejection = MKT(P_t)$. In other words, if the test value ($rejection$) of 1 indicates a rejection of the null hypothesis at α significance level, then a trend does not exist in the time series data (P_t) and vice versa. Figure 21 shows the procedure to pick the stationary window of data to perform FT. In a word, each spectral analysis should be done on the stationary window of data, MKT is the method to determine the length of the stationary window for t_i and t_m.

While using the MKT, the length of stationary windows where the pressure starts dropping at the initiation of the hurricane (t_i) and the pressure is at the minimum value (t_m) are determined (Figure 22). MKT testers are used in the analysis of hurricane Dorian and Isaias. The following is a flow chart to use the MKT tester:

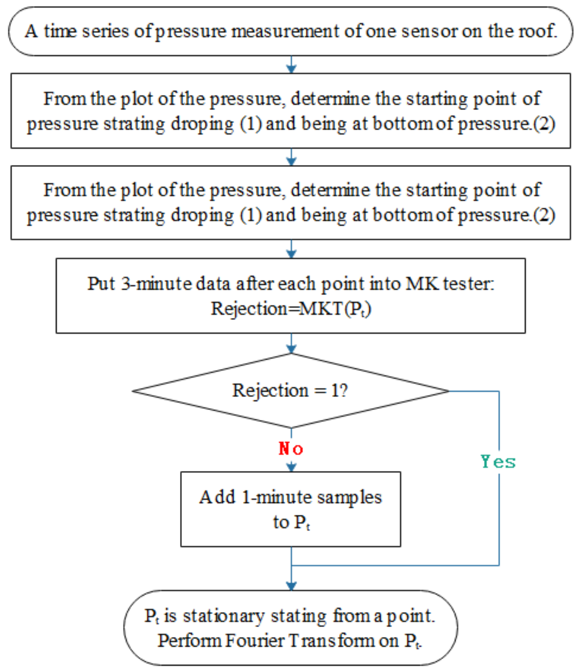

Figure 21 A Flowchart Showing Procedures of Determining the Stationary Pressure Data P_t

If $Rejection = 0$, P_t does not reach the critical length of stationarity, then we add 1-minute data to recheck the stationarity until $Rejection = 1$, P_t reaches to the critical length and is ready for spectral analysis. Due to the different locations of the sensors on the roof, the length of the stationary window is various. The shortest window length is chosen as the final stationary window.

Fourier Transform (FT) and Power Spectrum Density (PSD) .

The Fourier Transform converts the data in time domain to frequency domain, of which magnitude represents the dominant frequency of fluctuations present in the original data. Discrete Fourier transform (DFT) applies FT on the finite sequence of equally-spaced samples (fixed sampling rate).

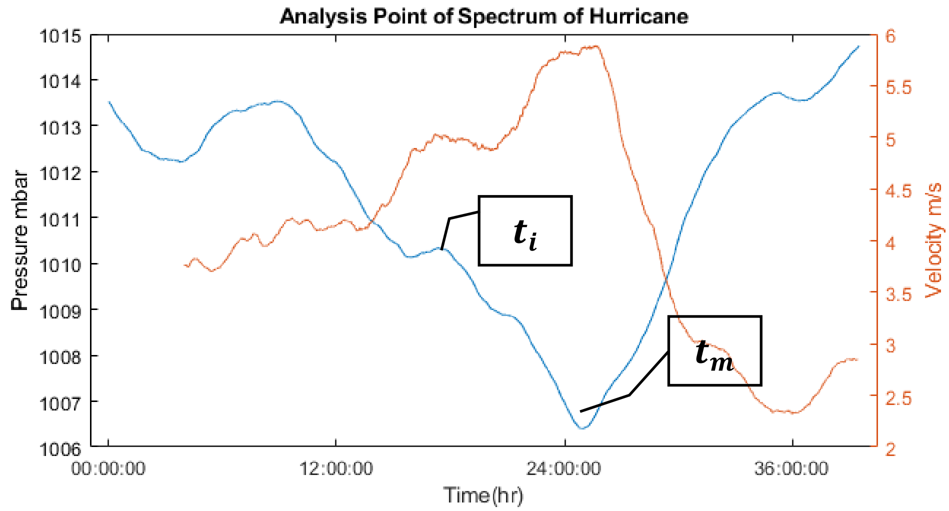

Figure 22 Hurricane Spectral Analysis Points.

Figure 22 shows the trend of pressure variation for a Hurricane. As for Euler's equation, $dp = -\rho v dv$. That is, the maximum pressure change occurs where the product of velocity and its gradient is minimum and vice versa. As is shown in Figure 20, the pressure starts dropping at t_i and reaches the minimum value at t_m. t_i and $t_m$are the time stamps for the spectral analysis of pressure data. The highest velocity gradient (0.5 $(m/s)/hour$), with 4.5 m/s mean occurs at the t_i . However, at t_m, the velocity gradian reaches $0(m/s)/hour, with$ 6 m/s mean. The highest velocity occurs where the wind direction is north-northeast. Due to the block of residential building and thick vegetation around Jack's house, the wind speed is lower than the record on the coast measured by National Hurricane Center by 10 to 15 m/s. Unfortunately, the data of wind speed and direction were not collected by the WSN system due to the connection problem of the anemometer during hurricane Dorian. The National Weather station data is shown in the plots together with the pressure variation plot.

PSD is a more common way to refer the spectral energy distribution. For the spectral analysis for the pressure at a stationary window, PSD is introduced as the unit of $mbar^2Hz^{-1}$. By comparing the PSD of pressure fluctuations at different locations on the roof, the frequency of the dominant wind fluctuations can be determined. The PSD at one frequency reflects the average energy content of the eddies. In addition, the distribution of different sizes (frequency) of the eddies in the flow determines the average kinetic energy of the fluctuations.

Chapter 4
Data Analysis and Results

Resolution Comparison

Pressure is one of the essential properties which are collected. Comparison of the resolution between the old and the new pressure sensor is determined by placing the new and old WSN pressure sensor in the indoor location. The actual pressure keeps more constant compared with the outdoor condition Figure 23. Figure 23 shows that the new system has less RMS, which is 0.05 mbar. The RMS of the old system is 0.52 mbar. While measuring under the same indoor environments, the RMS of the old system is around ten times larger the new system. The mean values from both WSN pressure sensors are the same, 1009.9 mbar.

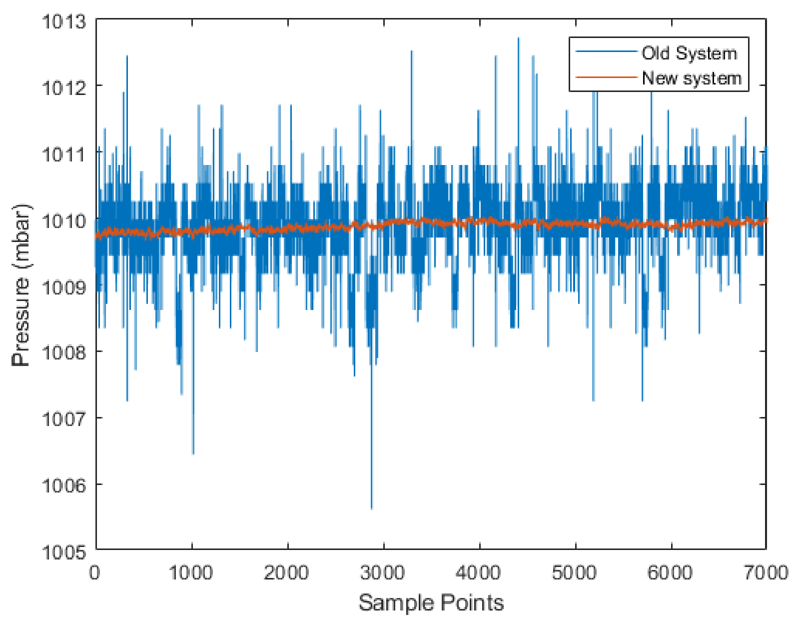

Figure 23 The Comparison of the Pressure Fluctuation Between New and Old System Measured at Indoor Condition

Pressure and Wind Variation Plots for Hurricanes

Isaias Plots of Pressure and Wind

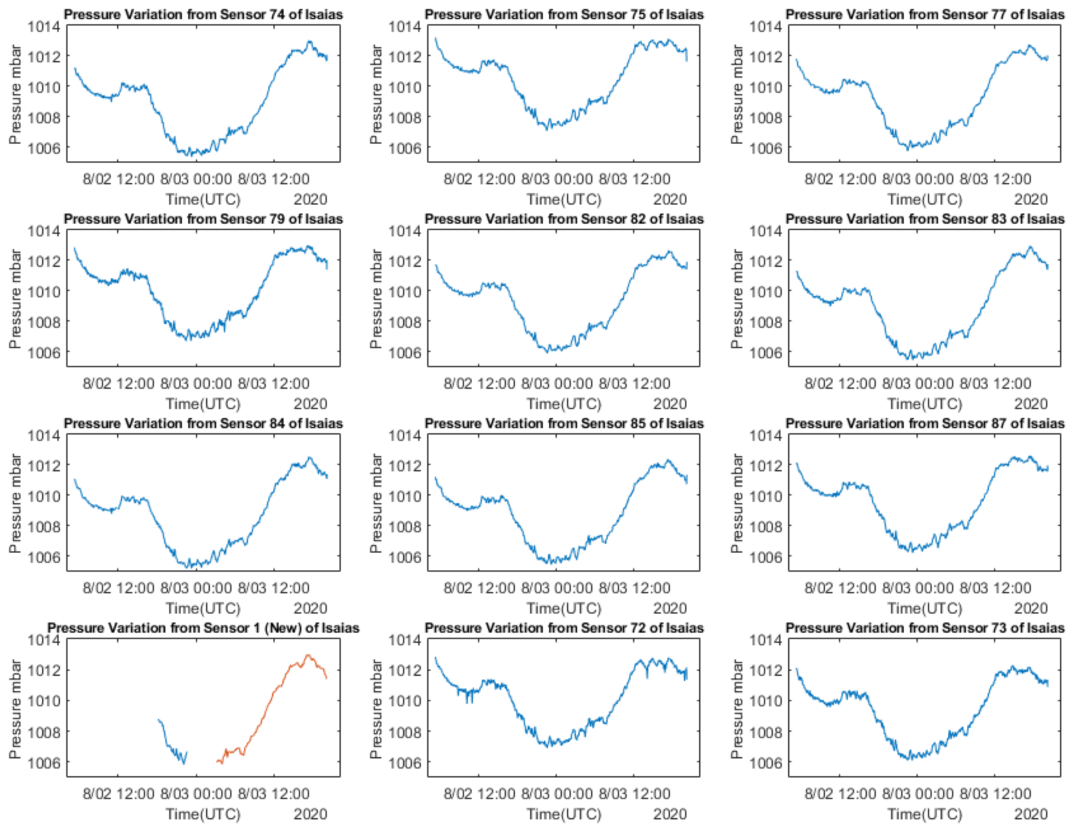

Figure 24 Pressure Plots from WSN Sensors during Hurricane Isaias

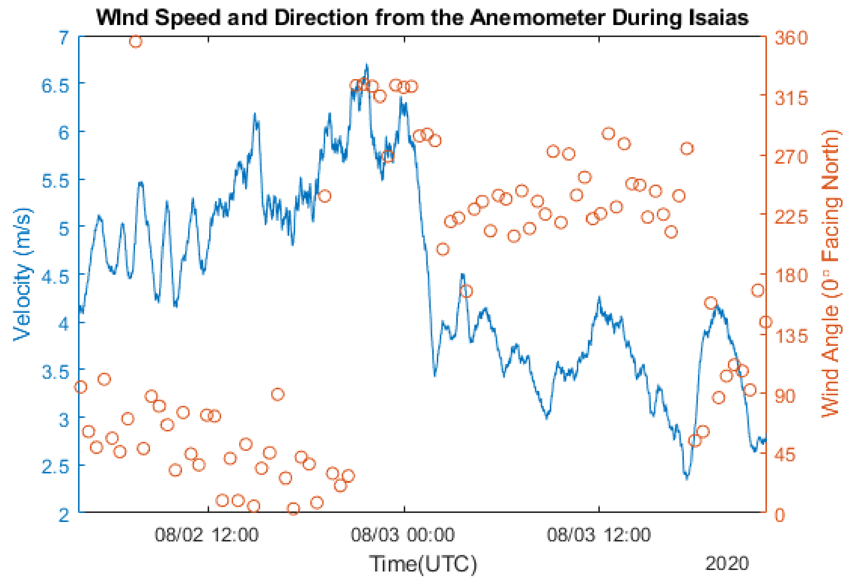

Figure 25 Wind Speed and Direction Measured by WSN Anemometer during Isaias

Figure 24 is the combination of 5-min MA pressure variation measured by the WSN sensor mounted on the roof of Jack's House. Except for sensor No. 1, all sensors were from the old WSN sensor. Figure 25 is the Wind speed and direction plots which were measured by the anemometer from the old WSN sensor. The wind speed and direction data were applied 5-min MA to get the clear trendline, where the scale of the direction in 0, 90,180, and 270 indicate north, east, south, and west.

Pressure started dropping from around 1011 mbar dramatically at UTC 1600 on August 2, 2020 and reached the minimum value of 1006 mbar at the rate of -0.75mbar per hour (Figure 30). The pressure stayed at the minimum value overnight until August 3 UTC 0230. During the midnight between August 2 and 3, the velocity also kept at the highest level, and the direction of the wind kept in the range of NNE to NNW (Figure 25). In the morning of August 3, the pressure increased, and the wind speed decreased at the rate of 0.33 mbar per hour and 0.38(m/s) per hour from NW (270°). Keeping increasing the pressure, the rate of the pressure changes increases to 1.1mbar per hour at UTC 0800 August 3, 2020. After UTC 1200 August 3, the pressure reached the value before the hurricane, and the wind speed keeps at 3m/s from east.

Dorian Plots of Pressure and Wind

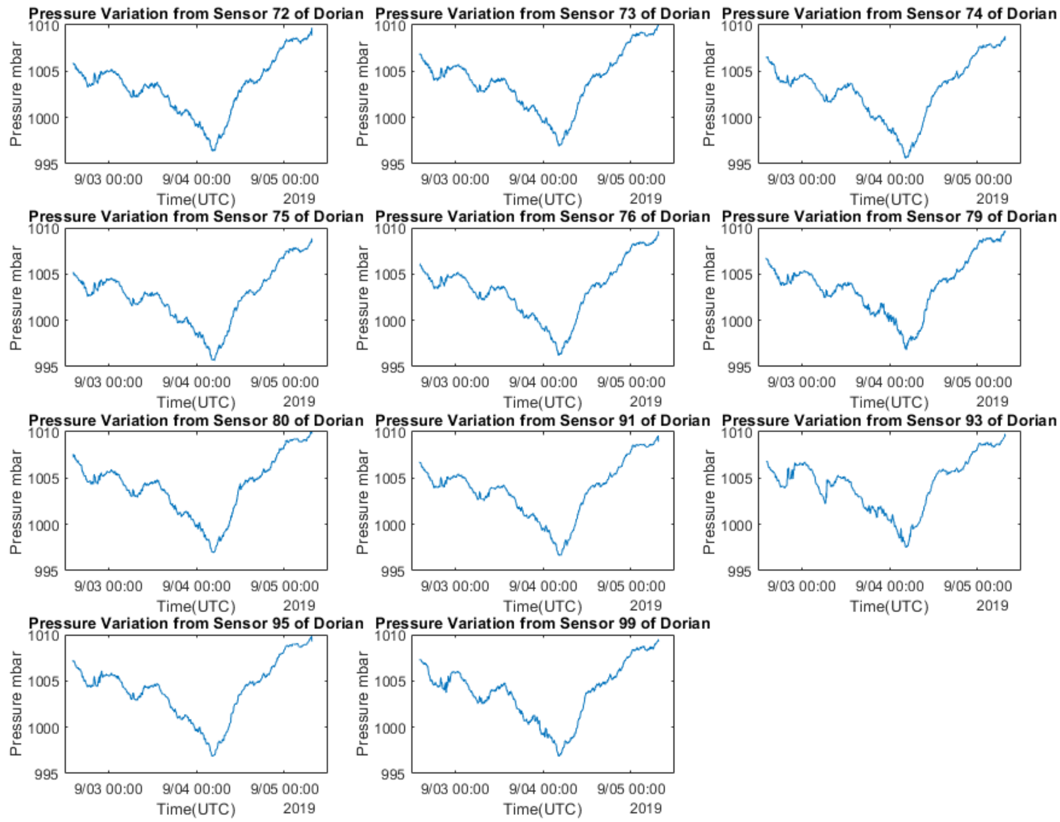

Figure 26 Pressure Plots from WSN Sensors during Hurricane Dorian

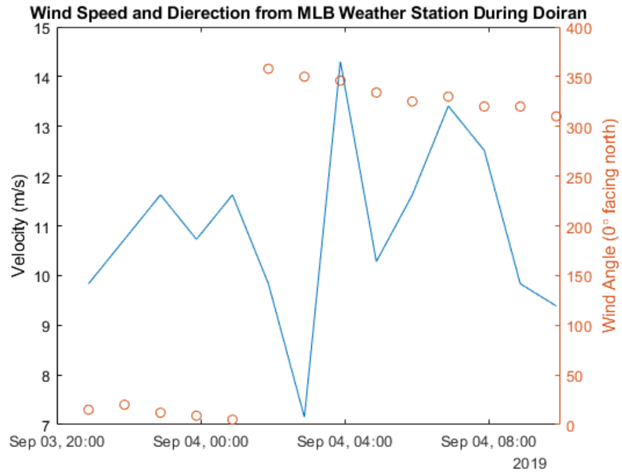

Figure 27 Wind Speed and Direction Measured by Local Weather Station during Dorian

Similar to the plots of hurricane Isaias, the dorian's plots is the combination of 5-min MA pressure variation measured by the old WSN sensors shown in Figure 26. Due to the connection problem of the anemometer during the hurricane, WSN system did not record the wind data. However, the data of the wind speed and direction is imported from the local weather station such as Melbourne airport (TWC, 2019), shown in Figure 27. Pressure started dropping from around 1003 mbar dramatically at UTC 1230 on September 3, 2019 and reached the minimum value of 997 mbar at the rate of -0.4 mbar per hour (Figure 26). Unlike the pressure of Isaias, the pressure of Dorian keep at the minimum value for only one hour (from UTC 0400 to 0500 on September 4) and rise very fast after that. In addition, wind speed is also reached to highest value (15 m/s from North to NNW). The wind gradually slowed down and a rate of -0.5(m/s) per hour from WNW. At UTC 1300 September, the pressure rises to the value before dropping at the rate of 1mbar per hour, when the wind speed decreased from the west.

Isaias Spectral Analysis

Two sampling time when the pressure starts dropping at UTC 1547 of August 2 and the pressure reaches the minimum value at UTC 2250 of August 2 (Figure 24). The length of the data to be spectral analyzed is 630s when pressure initially drop (called t_i) and 710s at

(t_m), which is determined by the MKT for each sensor. At t_i, spectral snalysis shows all potential fluctuation with 10Hz sampling rate. The spectral analysis on the pressure values along the east eave indicates the pressure frequency distribution on the PSD plot, in which the y-axis is PSD, and the x-axis is the frequency domine, as is shown in Figure 28. The range of the frequency axis is 0 to 0.14 Hz, where 0.07 Hz separates the frequency to lower and higher frequency. The sensor's location on the roof is shown in Figure 16(b). The corresponding sensor numbers are 74, 77, 82, and 84 of the houses, where sensors 82 and 84 are symmetric with the ridgeline (Figure 28a). Sensors 75, 79, 83, and 85 were located west of the sensors 74,77,82 and 84, respectively. An additional sensor 87 did not compare with any sensor at the inland area of the roof. Most of the power is distributed in the range of 0.02 to 0.12 Hz. Lower and higher subdomains are separated at 0.06 Hz. At the lower frequency domain, the size of the eddies of the flow is larger than those at the higher frequency domain. The PSD reflected the density of the eddies, which are related to the kinetic energy of the flow at a certain location. At the beginning of Isaias, the most power is contained in the lower frequency 0.02 to 0.06 Hz range as the flow reaches the middle of the ridge. At the t_m of the hurricane, the peak PSD appears to be at even lower frequencies, 0.01-0.03 Hz. This suggests that low-frequency large-scale motions contribute to most of the suction peak during the hurricane. For all inboard sensor locations, the frequency which occurs the maximum PSD value increases, suggesting more kinetic energy from intermediate scale eddy contributions to the pressure fluctuations typically of shear flows.

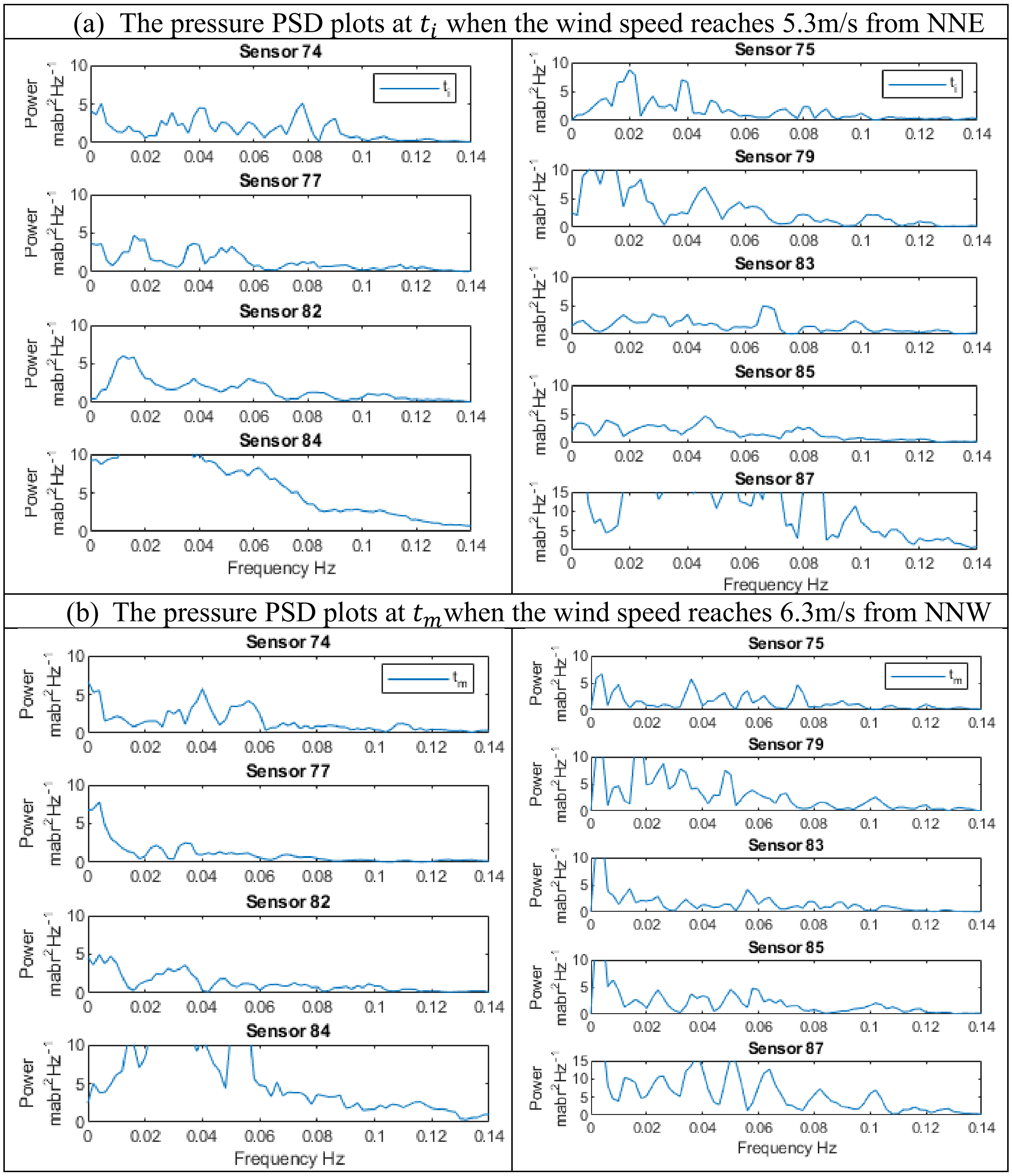

Figure 28 The Pressure Spectral Analysis of Sensors Installed at East Eave During Isaias-2020 at (a) $t_i$and (b) t_m

At t_i, the PSD peaks are shown at both lower and higher frequencies with sensor 74, which is near the NE roof corner. Also, the PSD at t_m in the higher frequency domain is less than the PSD of t_i by $5.3 - 2.1 = 3.2 mbar^2Hz^{-1}$. As is translated to the flow properties, both large and small eddies on sensor 74 contain a significant among of kinetic energy at t_i, whereas the small eddies are gradually merged to the larger eddies at t_m. For both sensor 77 and 82, located south of sensor 74 near the east eave, the larger eddies are dominant at both t_i and t_m, where maximum PSD are 4.7 and 2.4$mbar^2Hz^{-1}$. The PSD value at t_i are two times of which at t_m in the lower frequency domain. Through the sensor located windward on the sloped-up roof, the acceleration effect diminishes the smaller vortex, along with sensor 77 to 82 where the PSD of both sensors are lower than 1.5 $mbar^2Hz^{-1}$. For sensor 84, where the flow just passes over the ridge, the kinetic energy of the large eddies rises at both t_i (12 $mbar^2Hz^{-1}$ of maximum PSD) and t_m (14 $mbar^2Hz^{-1}$ of maximum PSD) due to the sudden separation at the ridgeline and the velocity decrement. Overall, the contributions of larger eddies are dominant along the eave on the east gable side.

When the flow is inboard of the roof, as shown in Figure 16(b), sensors 75 to 87 are spectrally analyzed. Due to the acceleration effect on the windward part of the roof, the vortex intensity at the t_m is diminished (Figure 28), shown in sensors 75 and 83 which the average PSD value are 6.1 and 3.5 $mbar^2Hz^{-1}$ for higher frequency domain. However, at sensors 75 and 79, the lower frequency contains the large PSD, 6.1 and 6.8 $mbar^2Hz^{-1}$ respectively. According to the shape corner vortex, the vortex effect is severe in the region near sensor 79 (Chowdhury, Moravej, & Zisis, 2019). The WOW testing model at FIU shows the corner vortex when the flow angle is 45 degrees (Chowdhury, Moravej, & Zisis, 2019). Instead, sensors 77 and 79 measure the noticeable flow fluctuation due to the corner vortex. The fluctuation occurs at sensor 85 and 87 at both t_i and t_m in the lower frequency domain and contain the average PSD of $4.5\ and\ 12\ mbar^2Hz^{-1}$. It is noticed that the PSD of sensor 87 settled far away from the ridgeline get the larger PSD of fluctuation than sensor 85 right after the ridgeline by $12 - 4.5 = \ 7.5mbar^2Hz^{-1}$.

(a) The pressure PSD plots at t_i when the wind speed reaches 5.3m/s from NNE

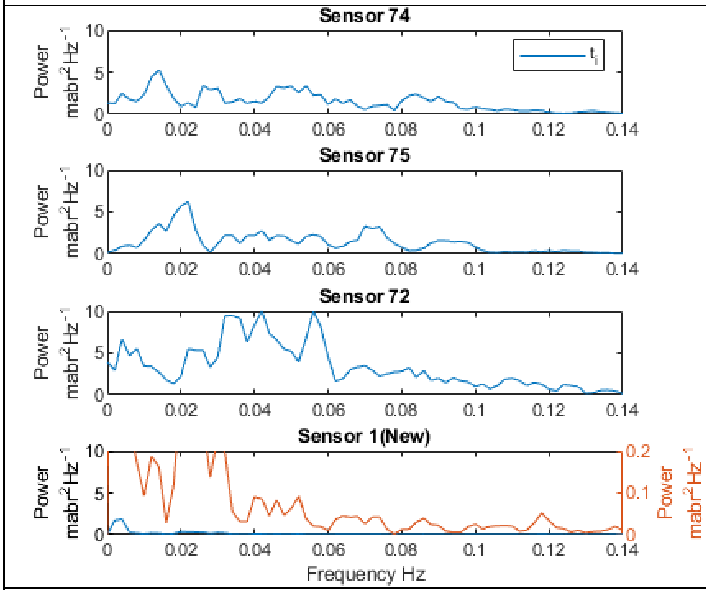

(b) The pressure PSD plots at t_m when the wind speed reaches 6.3m/s from NNW

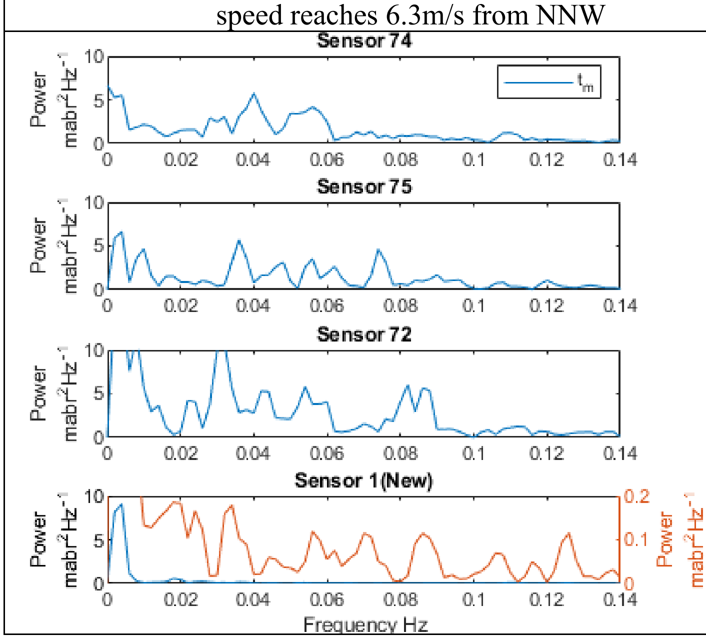

Figure 29 The Pressure Spectral Analysis of Sensors,74,75,72, And 1 Installed at the North Eave During Isaias-2020 at (A) t_iAnd (B) t_m

In Figure 29 sensors 74 to 72 belong to the old system, and sensor 1 belongs to the new system which generates the lower based electrical noise. Hence, the PSD scale of sensor 1 is lower than that of the old system. The PSD values are similar at t_i and t_m ,which suggests the relatively constant strength of the flow fluctuation on the north eave during the Isaias. The large eddies convert energy through sensor 74 to sensor 1 due to the increment of the PSD at the lower frequency domain, from the $4.5 mbar^2 Hz^{-1}$ of sensor 74 to $8.0 mbar^2 Hz^{-1}$ of sensor 72. However, peaks represent at the higher frequency domain, which indicates the small eddies, travels along the north eave at the average PSD of 5 $mbar^2 Hz^{-1}$.

Dorian Spectral Analysis

As in hurricane Dorian in 2019, the old system sensors were attached to Jack's house for obtaining enough data to perform spectral analysis. For hurricane Dorian, $t_i$and t_m are UTC 1230 on September 3 and 0400 on the following day. The result of the MKT values for t_i and t_m are 600 and 550 seconds. The wind data was not recorded by the WSN system but obtained by the Melbourne airport weather station. From the local airport data, the wind direction was approximately NNE (t_i) to the north (t_m) as the pressure dropped from t_i to the t_m. Sensors 72, 75, and 80, located on the east eave, are compared with the inboard sensors 73, 76, and 79. In addition, sensor 99, located on the leeward ridge, is to analyze the separation effect. Sensor 91 is located on the south eave. Same as hurricane Isaias, 0.07 Hz is the separating point between lower and higher frequency domain.

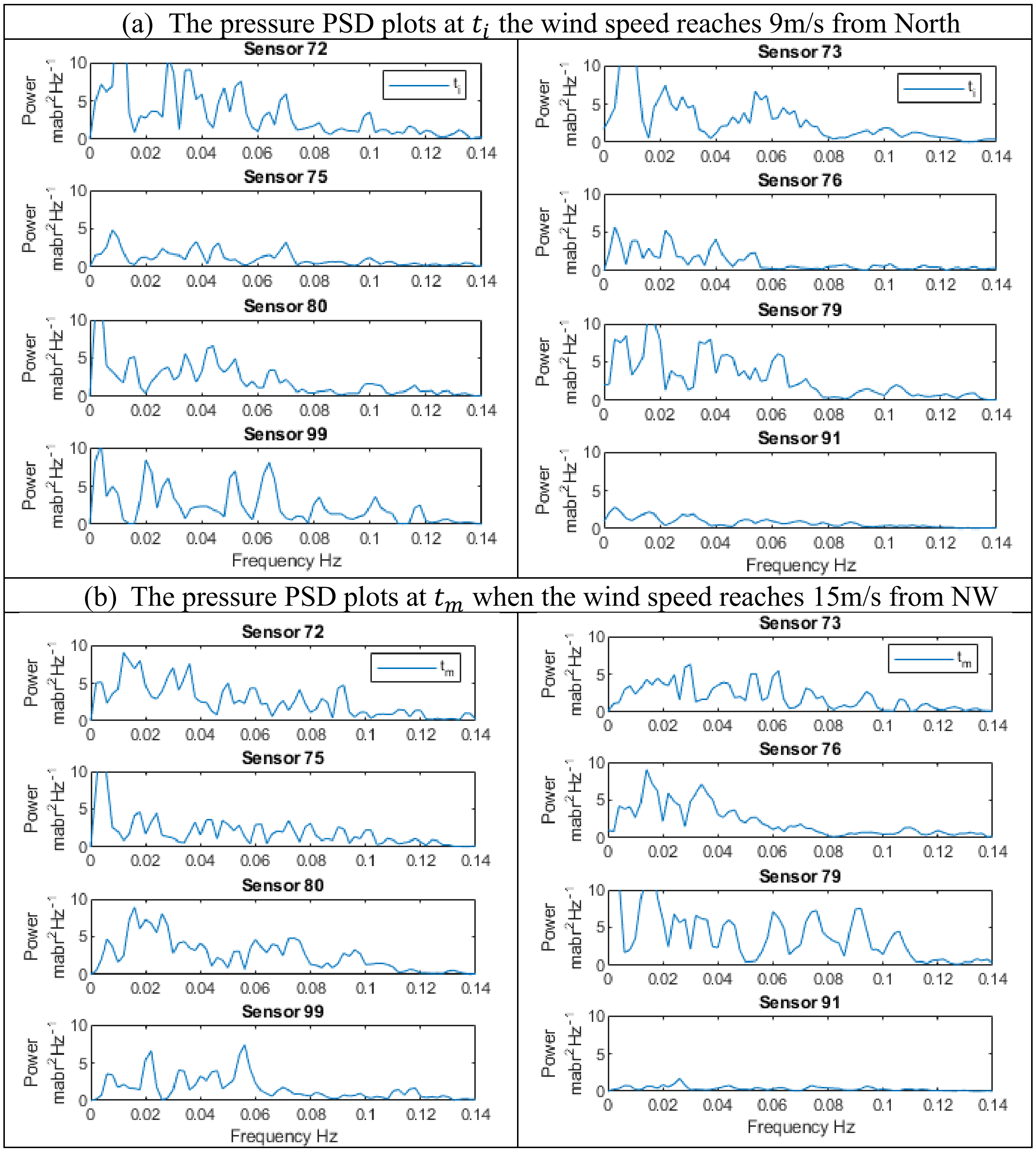

Figure 30 (a) The Pressure Spectral Analysis of Sensors Installed at East Eave during Dorian-2019 at (a) $t_i$and (b) t_m.

In the higher frequency region, from sensor 72 to sensor 80 in front of the ridge, the fluctuation of the flow is diminished gradually for t_i and t_m, shown in Figure 30a. The acceleration effect of the flow cascades the vortex energy to the higher frequency (small eddies) in the area between sensor 72 and sensor 75, and the lower frequency vortex (large eddies) keeps the strength until sensor 80 with 7.5 and 5.5$mbar^2Hz^{-1}$ of the average PSD at the t_m and t , due to the high PSD in the lower frequency region, which indicates the fluctuation of the flow has a slight strengthening. At t_m, the smaller eddies remain dominant at the windward side of the roof. For sensors 72, 75, and 80, the maximum value of the lower frequency domain at t_i are 11.5, 5.2, 8.8, and 10.1 $mbar^2Hz^{-1}$, and 8.5,4.8,9.0 and 6.8 $mbar^2Hz^{-1}$ at t_m. At the leeward side of the ridge, at the location of sensor 99, the separation effect acts on the large eddies (lower frequency domain) where the PSD value is 10.2 for t_i and 7.5 $mbar^2Hz^{-1}$ for t_m. Compared with the PSD plot of sensor 84 (separation effect) of Isaias, sensor 99 of Dorian at the same location PSD is decreased by 1.1 $mbar^2Hz^{-1}$. At the inboard area of the windward roof, the acceleration effect acts on the arer from sensor 73 to sensor 76, but not on sensor 79, in Figure 30b. On sensors 73 and 76, the PSD keep at the low value (<3 $mbar^2Hz^{-1}$) at higher frequency domain for both at t_i and t_m, which shows large eddies convert the kinetic energy. The maximum PSD at both frequency domains of sensor 79 increase to 10 and 7 $mbar^2Hz^{-1}$ for t_m. However, at t_i its maximum PSD at high frequency keeps less than 4 $mbar^2Hz^{-1}$. Unfortunately, there are no more sensors attached on the leeward side of the ridge, apart from sensor 91 at the south eave. The separation effect after the ridgeline is not recorded. A rare vortex of flow is shown at sensor 91, and little value is on the PSD plot both at t_i and t_m. Because of the block of the trees and houses, the flow effect is hard to act on the location of sensor 91.

Two sensors are located at the north eave, sensors 72 and 73, and one sensor 95 is located at the inboard area of next to sensor 94 (Figure 16). Sensor 94 lost connection during Dorian and rare data were recorded. The vortex intensity decreases from east to west in the major form of large eddies (low frequency) (Figure 31). At the northeast corner, the effect of the corner vortex is more noticeable at sensor 73, which contains the large eddies, with the maximum PSD of11.0 $mbar^2Hz^{-1}$ at t_i and 7.2 $mbar^2Hz^{-1}$ at t_m, than at sensor 72, with the PSD of 10.1 $mbar^2Hz^{-1}$ for t_i and 4.6 $mbar^2Hz^{-1}$ at t_m. A little number of the small eddies were shown on the PSD plots for sensor 72 and 73, with the maximum PSD of 5 $mbar^2Hz^{-1}$. The acceleration effects on sensor 95 causes the noticable decrement of PSD on the whole frequency domain for both t_i and t_m.

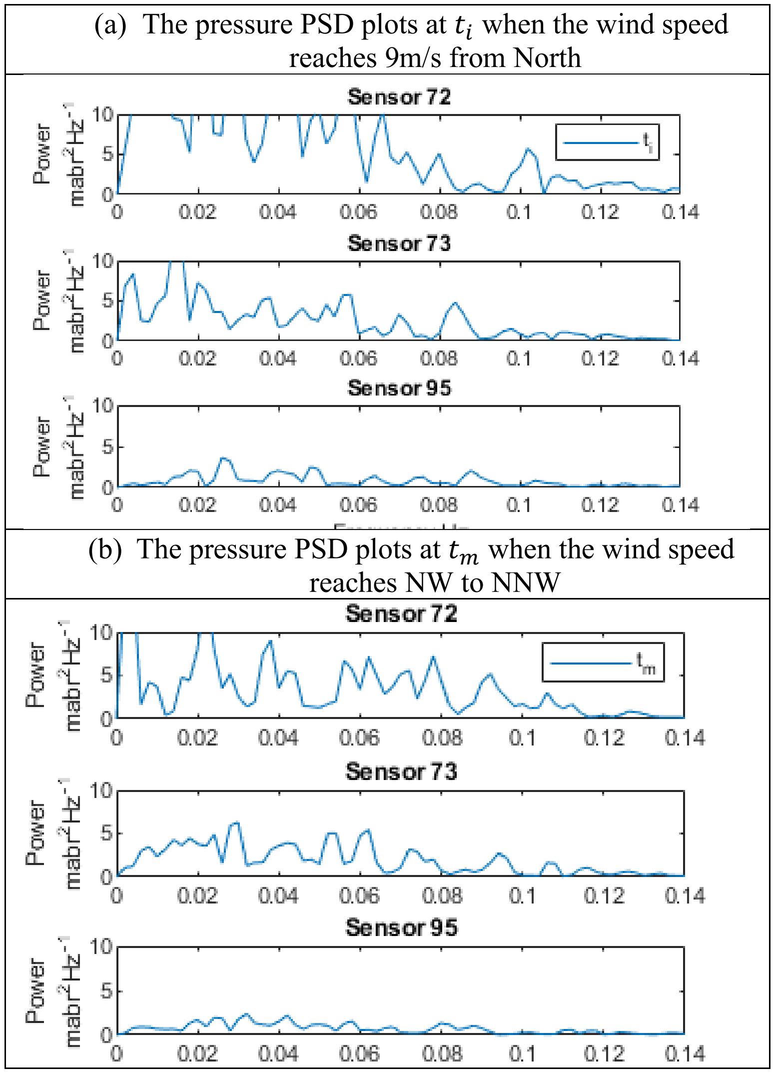

Figure 31 The Pressure Spectral Analysis of Sensors 72 and 73 Installed at North Eave during Dorian at (a) t_i and (b) t_m

WOW Spectral Test

To verify observation during a natural hurricane, a spectral analysis focusing on the roof is necessary. The flow angle is 45°, and the speed is 60mph, which is to simulate the corner vortex of the windward roof corner. 45° of flow angle is determined by the average wind direction recorded by the anemometer and weather station from the t_i to t_m of both nature hurricanes.

The Sensors 27, 26, 25, 23, 22, and 21 were attached at the north eave of the gable shown in Figure 34a. Sensors 31, 30, 24, 29, and 28 are located at the inside area of the gable, shown in Figure 34b. Sensor 27, 31, and 34 are at the east eave, shown in Figure 35. The range of the frequency is from 0 to 0.6 Hz on the spectral plots, where the separation line of the lower and higher frequency region is 0.3 Hz. The virtualization of corner vortices on a horizontal roof (Figure 32) by Arindam shows the potential vertices distribution along the edge of roof (Chowdhury, Moravej, & Zisis, 2019).

Figure 32 Corner Vertex Visualization by Chowdhury

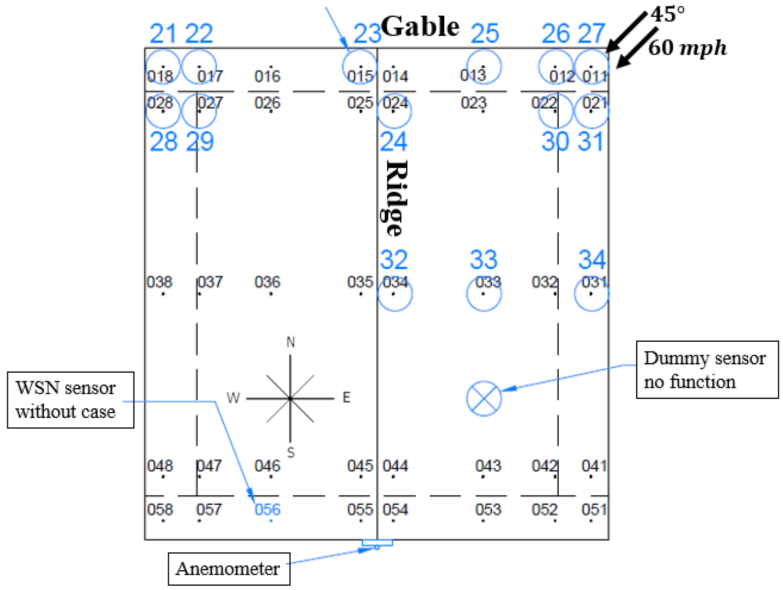

Figure 33 The Roof Sensor Attachment Detail, Including Test Wind Speed and Direction.

The acceleration of the flow diminishes the vortex intensity on the windward roof. At sensor 25, the corner vortex effect is obviously reflected by the increment of the PSD at the entire region of the frequency, shown in Figure 34a. At sensor 25, located on the inboard area of the leeward edge near the gable, the fluctuation of the flow rises up (Figure 34a), which causes the minor rising of the PSD. The separation effect occurs right after passing the ridge of the roof, reflected on sensor 23, and the power of the entire frequency domain increases. The separation of the flow also strengthens the fluctuation of the flow, which is gradually eliminated until sensor 21.

At the inside area near the north eave, the acceleration effect decreases the fluctuation of the flow from sensor 31 to sensor 24, shown as Figure 34b, where the PSD at the entire frequency is diminished. The separation effect is not noticed because no sensor was installed on the leeward side of the ridge. The modest increment of the PSD for the entire frequency domain indicates the strength increment of the turbulence under the corner vortex effect.

Spectral analysis for three sensors at the east eave of the roof shows in Figure 35. An increasing number of the smaller eddies are viewed in the spectral plot of a higher frequency domain along with sensors 27 and 31. However, smaller eddies are not noticed when it flows south with the lower PSD value at high frequency. The larger eddies remain strong through the east eave. The acceleration effect at the windward roof and separation effect at the leeward side of the ridge has been proved at experimental hurricanes compared with hurricane Isaias-2020.

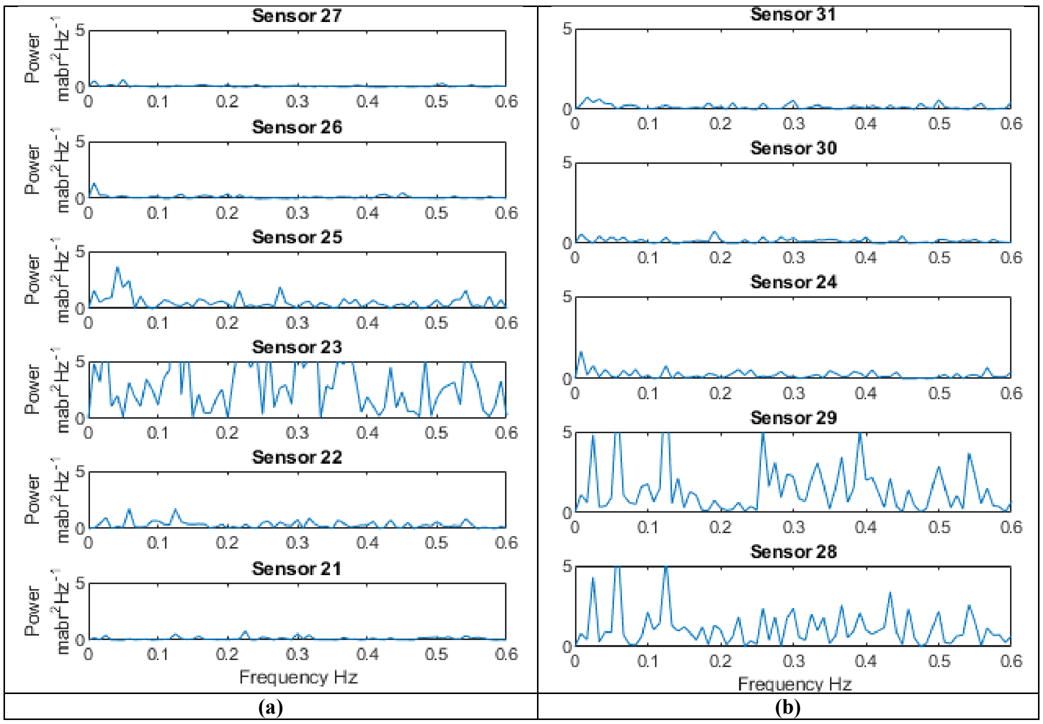

Figure 34 (a) The Pressure Spectral Analysis of Sensors 27 to 21, Installed at North Eave during WOW-2020 (b) The Pressure Spectral Analysis of Sensors, 31 to 28 Installed the Inside Area Near the North Eave on WOW-2020, 45° at 60 mph

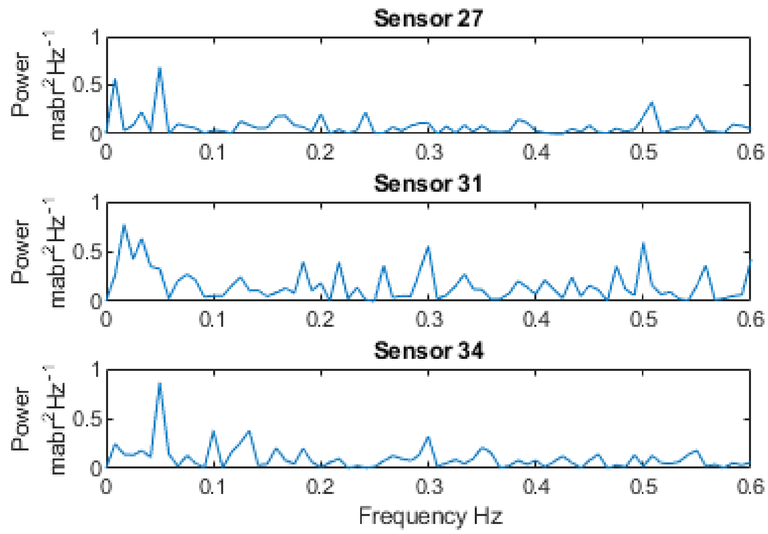

Figure 35 The Pressure Spectral Analysis of Sensors, 27, 31, and 34, Installed at East Eave During WOW-2020, 45° at 60 Mph

Chapter 5
Conclusions

The new WSN system improves the accuracy significantly compared with the Old system (Figure 23). The ideal resolution of pressure and wind speed measurement is 0.1 mbar and 0.05m/s, due to the upgraded 16bit ADC with the oversampling technic. The answer of humidity, temperature, and wind direction are improved, which are 0.03%RH, $0.05°C$ and 0.005 degree respectively. Keeping the similar structure of the old WSN system, the new WSN system also updates the Xbee module to 3rd generation work in the Zigbee network. The Velcro attachment method can keep the sensor safe when the speed is no more than 40.2 m/s (90mph), which is one of the testing results from WOW. In addition to collecting and save data from sensors, the new-designed software synchronizes the data to the DisignSafe.

The trend of the pressure variation for both hurricanes was compared. First, the pressure dropping range for both hurricanes can be analyzed. For hurricane Dorian, the pressure dropped from 1007 to 996 mbar (decrement of 11mbar). The pressure drop range of Isaias is from 1011 to 1005 mbar, which is a decrement of 6 mbar. Second, the period that the minimum pressure keeps indicating the moving speed of hurricanes. It takes five hours for Isaias to stay at the minimum value of the pressure but one hour for Dorian. This reflects a higher moving speed that Dorian obtains than Isaias does, which is proved by the hurricane reports by NOAA (Avila, Stewart, Berg, & Hagen, 2019; Bullentin, 2020).

An ever-changing wind (direction and speed) and the surroundings (buildings and plants) affect the pressure measurement and affect the pressure's spectral plots more unpredictable. In contrast, the objectives-oriented experimental test keeps relatively constant wind speed to emphasize the phenomenon, leading to the purified spectral properties or pressure.

Comparing spectral analysis for two different category hurricanes, Dorian and Isaias, and an experimental test (WOW) indicates the similar pressure fluctuation properties reflected on PSD plots of pressure at the beginning of hurricane and peak minimum pressure region. The based noise of the new WSN system is less than that of the old WSN system, reflected on the tick values of the PSD axis on spectral plots of new and old WSN systems. The spectral analysis focus on the pressure acting on the windward, leeward, and ridge, with the effects of acceleration, separation, and corner vortex. The qualitative comparisons and similarities of PSD at different sensor locations among other hurricanes and WOW tests are analyzed with the PSD plot. However, within a WSN system, the dominant spectral area is relevant to the location of the measurement on the roof. On the windward and gable side, the acceleration of the flow, due to the sloped-up top and the wind directions, decreases the eddy development before the ridge, shown on the lower frequency region of spectral plots. This effect shown at hurricane Isaias matches better with the WOW result than that at hurricane Dorian. Because on Dorian and WOW PSD plots, the sensors located at the windward roof show the smaller values of PSD than the sensor located behind the ridgeline at the lower frequency domain. The separation effect at the location right after the ridge of the flow generates the disturbance of the flow associated with the increment of PSD distributing on the frequency domain. This effect shown at hurricane Isaias matches better with the WOW result. Because, as for the sensors behind the ridgeline on both Dorian and WOW, the PSD increases significantly on the lower frequency domain. The corner vortex effect acts on another right-angle side of the roof, neither as attenuated as acceleration effect on the windward gable side nor as enhanced as separation effect just after the ridge. Both hurricanes match this effect with experimental results well, especially at the middle point of the gable side eave. Both field and experiment results prove that the vortex strengthens the fluctuation of the flow and increases the PSD of pressure over the frequency domain. Arindam's visualized corner flow in the WOW is tested in WOW in a flow on a non-looped roof at 45°, shows that the vortex develops along two windward edges and approves the conclusion above. (Chowdhury, Moravej, & Zisis, 2019). The vertex presents at the corner of the roof. It develops two conical structures, where the WSN sensors were installed around conical structures as the similar situation of hurricanes and the WSN WOW test (Figure 32). The contour of the peak pressure coefficient $C_{p\,min} = P_{min} / 0.5\rho v^2$ recorded the worst chaos condition of the flow and reflected the vertices in this scenario (Chowdhury, Moravej, & Zisis, 2019). P_{min} is the minimum (negative peak) of pressure measured at the sensros, ρ is the density of air ($1.225 \mathrm{kg/m^3}$), v is the wind speed of the test. On his research, $C_{p\ min}$ indicate the pressure fluctuation on the roof which is place horizontally. The low $C_{p\ min}$ area shows that the vertex drops the pressure along the conical structure on the roof (Figure 36). The lower $C_{p\ min}$ means the higher power of corner vertex. In Figure 36, the x-axis shows the direction that the sensors were placed during the WOW test. Along the x-axis, Arindam's $C_{p\ min}$ increasing from -6 to 0.5. Figure 37 is the plot of $C_{p\ min}$ value WOW test at 45° and 60 mph. L/L_0 is the coefficient of length, where L_0 is the total length of the north eave of the house model. The $C_{p\ min}$ decreases until L/L_0 = 0.6 and raches the minimum values of -1.3. Then, it starting increases to -0.3 of $C_{p\ min}$ at L/L_0 = 0.9. Due to the shape the roof, the acceleration effect on the windward roof limits the effect of the vertices until the rear of ridge line, As it is far away from ridgeline, the separation effect together with the vertices is not as strong as before and increase the $C_{p\ min}$ at the leeward side.

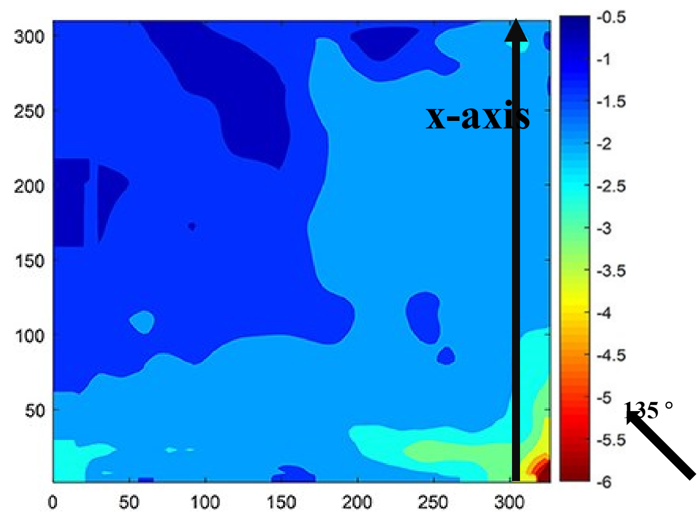

Figure 36 Contour of $C_{p\ min}$.

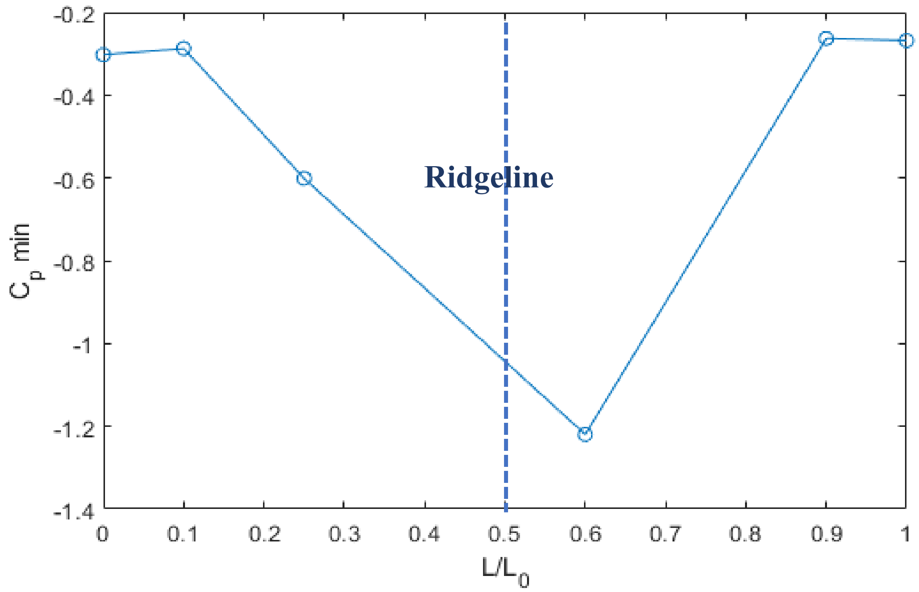

Figure 37 The $C_{p\,min}$ Plot of the North Eave Sensors 27, 26, 25, 23, 22, and 21 During the WOW 45° 60mph

Since 2018, there were a huge amount of data measured during the hurricane season. After the measurement, it takes a long time to work on the raw data for various academic aims. Hence, I have learned a lot from each time processing WSN data. First, it is necessary to record every small work and event during the measurement, especially the deployment period. Every small event done during that time may act as a hint to solve the potential problem. Due to the complete event was of WOW, the maximum wind speed of Velcro is analyzed after the WOW. Second, synchronize the time of the computer with the local time. It took a long time to fix the wrong timestamps that were recorded during Dorian and Isaias. Third, as the sensor cases still occupy some space, the effect of casing on pressure measurement is non-negligible, which needs maller cases to connect the sensor board with a more negligible effect on the flow. Finally, as for the WOW test, 1 min window is too short for the spectral analysis for a fixed angle and wind speed. As WSN sensor measures ten samples per second, only 60 seconds (600 samples) of data is recorded for each test. Compared with the length of the stationary window from nature hurricanes, from 400 seconds to 600 seconds, the test duration needs to be improved to reach the level of stationary windows from natural hurricanes.

References

Alfonso, F., & Hayes, M. (2019). *CNN.com*. Retrieved 9 4, 2019, from https://edition.cnn.com/us/live-news/hurricane-dorian-us-florida/h_6e95b414fc7b5f4c6f2dda730f061db0

Aly, A. M., Bitsuamlak, G., & Chowdhury, A. G. (2011). Florida International University's Wall of Wind: a tool for improving construction materials and methods for hurricane-prone regions. *Vulnerability, Uncertainty, and Risk*, 352-359.

Avila, L., Stewart, S., Berg, R., & Hagen, A. (2019). Huriicane Dorian. *National Hurricane Center Tropical Cyclone Report*. Retrieved from National Hurricane Cneter Tropical Cyclone Report: https://www.nhc.noaa.gov/data/tcr/AL052019_Dorian.pdf

Bendat, J. (2011). Random Data: Analysis and Measurement Procedures. *John Wiley & Sons*, 566.

Beven, J. (2020). *Tropical Weather Outlook.* Miami: National Hurricane Center.

Bullentin. (2020). *Tropical Storm Isaias Advisory Number 24.* Miami FL: National Hurricane Center.

Chowdhury, A. G., Moravej, M., & Zisis, I. (2019). Mitigation of Aerodynamic Uplift Load. *Frontiers in Built Environment*, 10. doi:10.3389/fbuil.2019.00010

Coch, N. K. (2020). Inland Damage from Hurricanes. *ournal of Coastal Research*, 1093–1105. doi:10.2112/JCOASTRES-D-20A-00002.1

Fatichi, S. (2009, October 09). *Mann-Kendall Test.* Retrieved 3 25, 2021, from https://www.mathworks.com/matlabcentral/fileexchange/25531-mann-kendall-test

Holland, G. J. (1980). An Analytic Model of the Wind and Pressure Profiles in Hurricanes. *Monthly Weather Review*, 2003-2013. doi:10.1175/2008JPO3727.1

Kelman, I. (2016). Saffir-Simpson Hurricane Intensity Scale. *Encyclopedia of Natural Hazards*. doi:10.1007/978-1-4020-4399-4

Kendall, M. (1979). The Advanced Theory of Statistics. *Macmillan Publishing Co. Inc.*, 748.

Lapillia, G., Chandiramanib, J., Kostanicc, I., Pinelli, J.-P., & Subramaniane, C. (2010). *New Wireless Sensors System for Pressure Measurement.*

Lee, D. (2020, 3 25). *Grafana 7.5 released: Loki alerting and label browser for logs, next-generation pie chart, and more!* Retrieved from Grafana: https://grafana.com/blog/2021/03/25/grafana-7.5-released-loki-alerting-and-label-browser-for-logs-next-generation-pie-chart-and-more/

Mann, H. B. (1945). Nonparametric Tests Against Trend. *Econometrica*(13), 245– 259.

Mazzei, P., & Bogel-Burroughs, N. (2019, September 4). *Hurricane Dorian Brings Surge Threat From Florida to Carolinas: Live Updates*. (The New York Times)

Pasch, R. (2020). *Hurricane Isaias Intermediate Advisory Number 15.* Miami, FL: National Hurricane Center.

Pasch, R. (2020). *Tropical Storm Isaias Discussion Number 7.* Miami: National Hurricane Center.

Ramage, C. S. (1959). Hurricane development. *Journal of Atmospheric Sciences*, 227-237.

Schott, T. (2019, 1 2). *National Hurricane Center and Central Pacific Hurricane Center.* Retrieved from https://www.nhc.noaa.gov: https://www.nhc.noaa.gov/aboutsshws.php

Stewart, S. R. (2020). *Hurricane Isaias Advisory Number 18.* Miami, FL: National Hurricane Center. Retrieved from https://www.nhc.noaa.gov/archive/2020/al09/al092020.public.018.shtml?

Stewart, S. R. (2020). *Tropical Storm Isaias Discussion Number 19.* Miami, FL: National Hurricane Center.

Sun, J., & Wang, J. (2020, 6 26). *HurricanHouse*. Retrieved from Github: https://github.com/sun128764/HurricaneHouse

TWC. (2019, 9 4). *Melbourne, FL Weather History-Orlando Melbourne Airport Station*. Retrieved from Weather Underground: https://www.wunderground.com/history/daily/us/fl/melbourne/KMLB/date/2019-9-4

Appendix

Appendix A:

WOW Sensors Test Layout

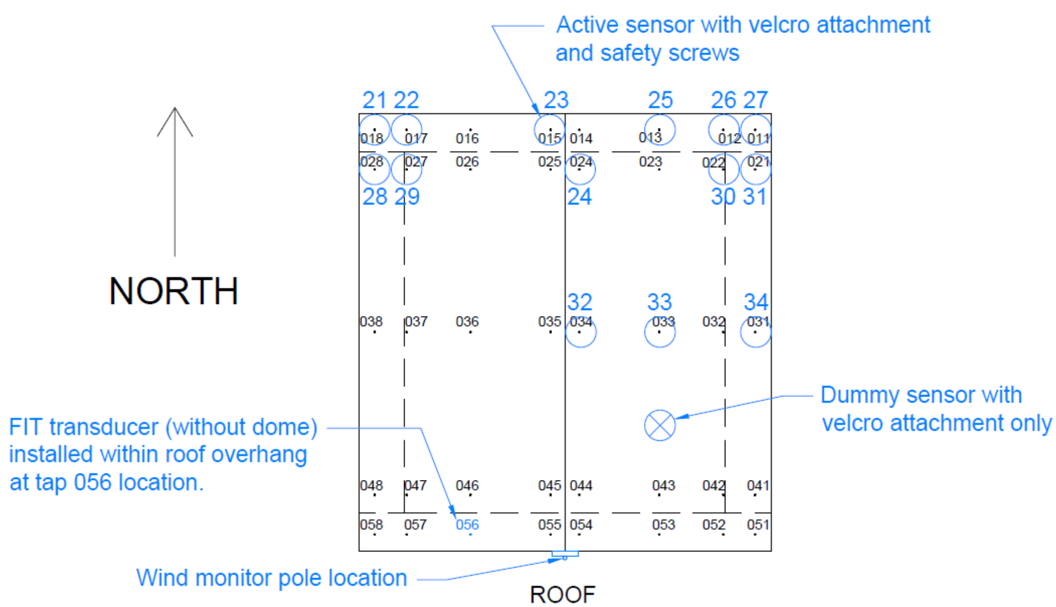

Figure 38 Sensors Layout on the Roof

Table 5 WSN Sensors List Corresponding to the Scanivalve Taps Number

Tap Locations	Sensor #	Note Only During the Deployment	Comparable Tap
Roof			
018	21		051
017	22		052
015	23		054
024	24		045
013	25		056
012	26		057
011	27		058
028	28		041
027	29		042

022	30		047
021	31		048
034	32		035
033	33		036
031	34		038
North Wall			
142~162	35		332
192	36		351&112
194	37		352&114
East Wall			
431	38		232[1]
451	39		411&252
452	40		412&253
Soffit			
516	41		571
512	42		575
511	43		576
541	44		542
South Side	Anemometer 101	BOX in 573	
In Door			
In Door South Wall	11[2]		None

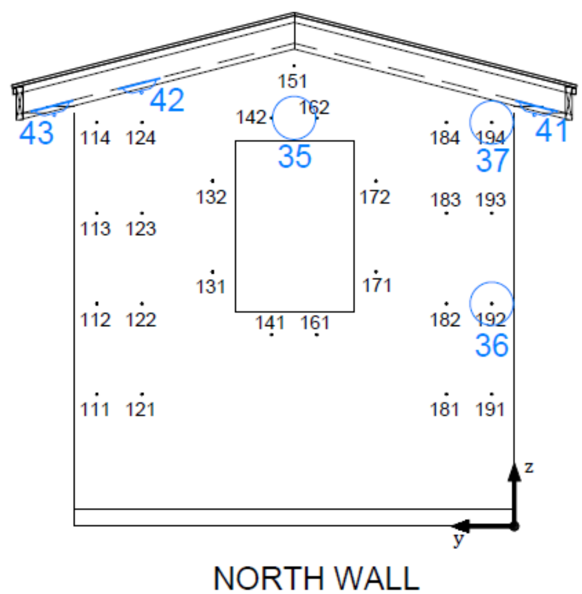

Figure 39 Sensors Layout on the North Wall

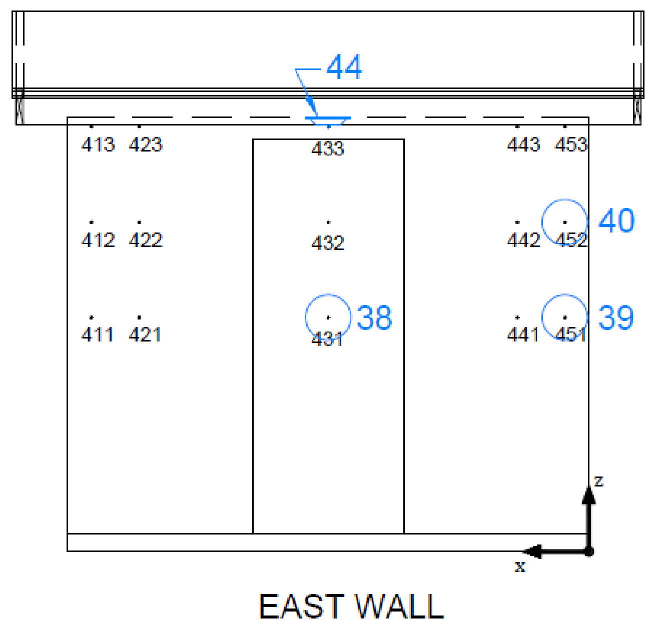

Figure 40 Sensors Layout on the East Wall

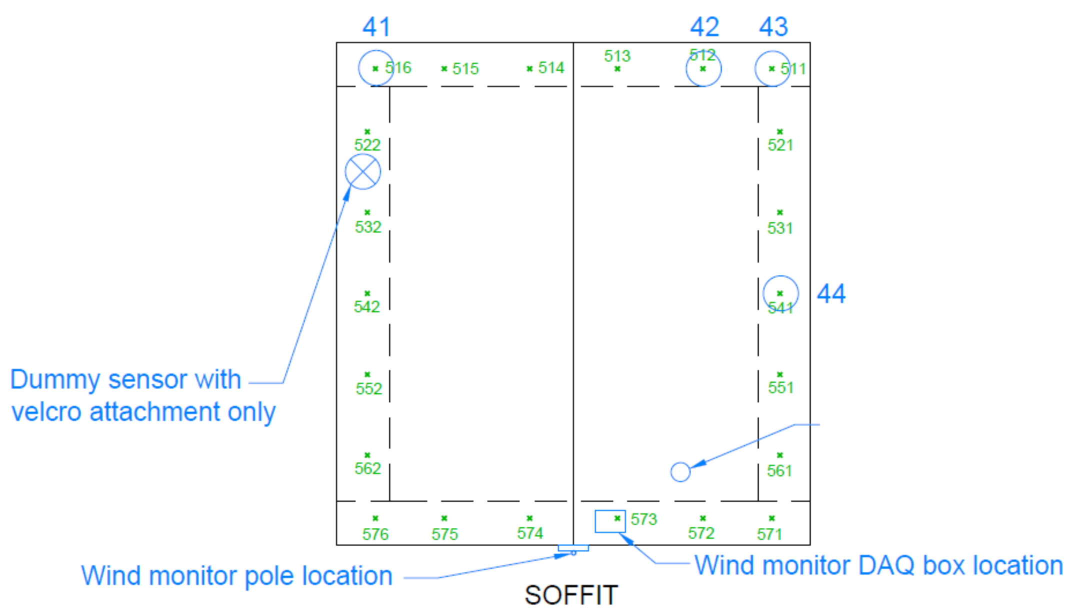

Figure 41 Sensors Layout on the Soffit

Appendix B:
Development of New System

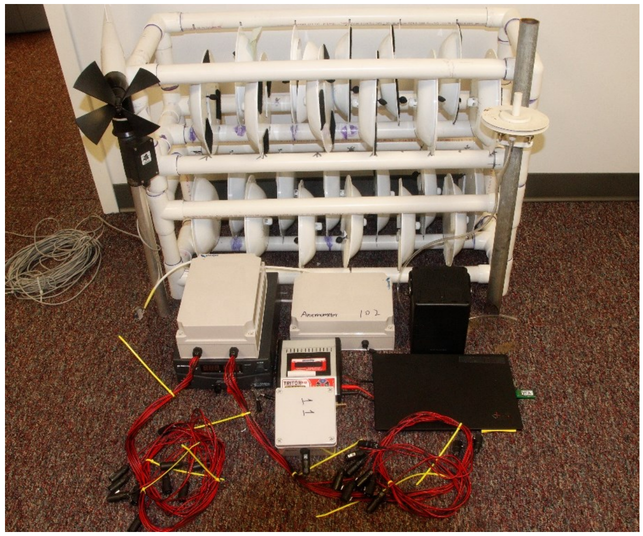

Figure 42 The System Photo of the New WSN System

Figure 42 shows the 24 pressure sensors, reference pressure, disk probe, anemometer, anemometer box, charging system, base unit, and laptop. The WSN sensor transmits the data to the base unit, which is connected to the laptop through COM. The circuit board measures data using the onboard sensors (pressure and temperature sensor) and sensor connected to the expansion port (anemometer, humidity, wind speed, and direction), shown in Figure 43. Jaycon System INC designs the circuit board (Figure 44) based on Adafruit Feather M0, which is supported by Arduino Integrated Development Environment (IDE). Arduino IDE helped us to develop functions very quickly with some open source libraries. This circuit board has a Li-ion battery pack to support it for 2 to 3 days without an external power supply. This board also support solar panel. The cases and boxes protest the electronic components from the extreme weather There are aviation connector ports on the cases and boxes for external charging power supply, data transfer, and on-off switch. (Figure 45). Figure 46 and Figure 47 show the pin-out connection detail of sensor casing and anemometer box.

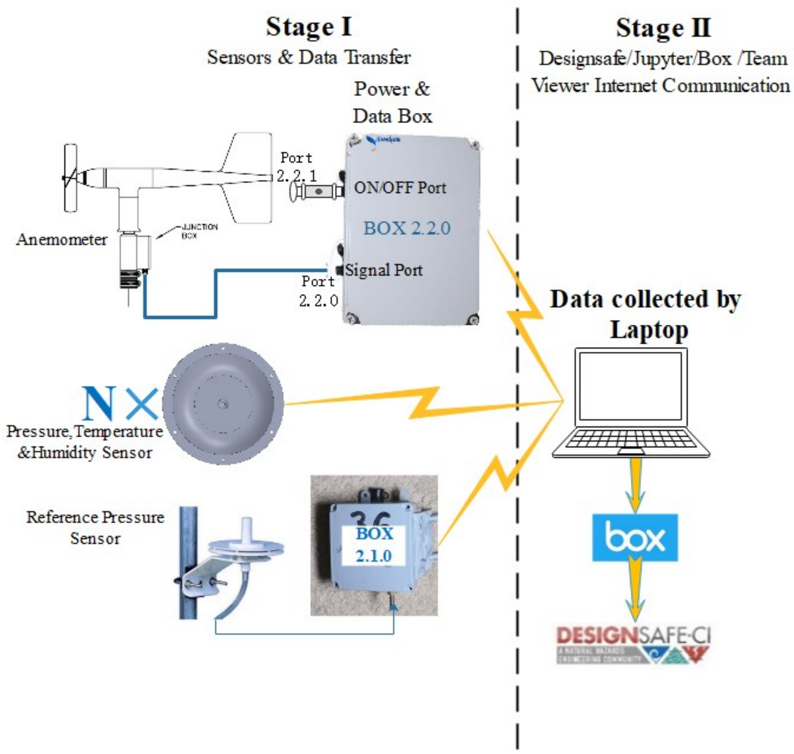

Figure 43 Architecture of the WSN Measurement System

Figure 44 The Circuit Board

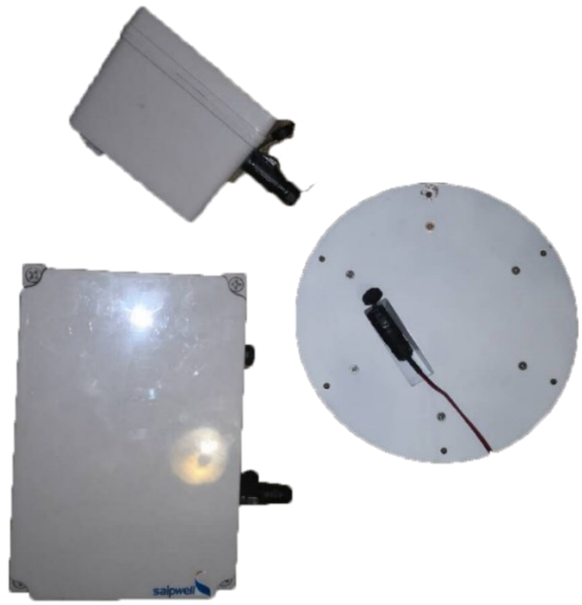

Figure 45 View of a Pressure Case (Right), Reference pressure box (top left) and Anemometer Box (Bottom Left)

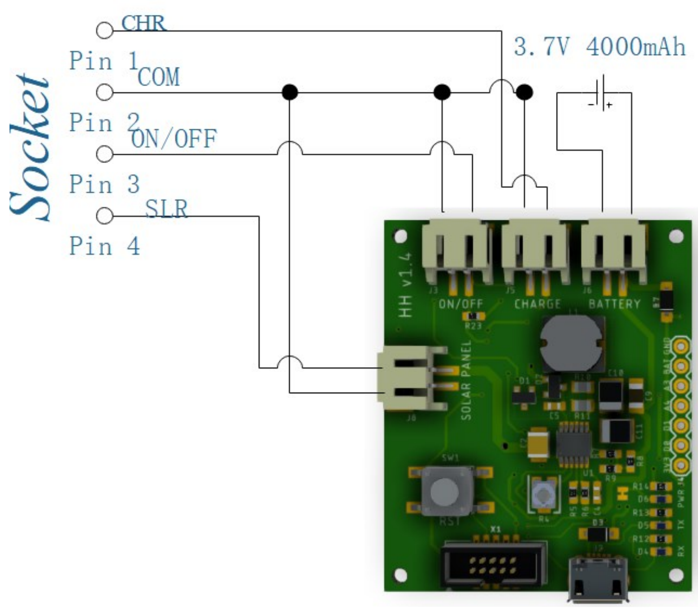

Figure 46 Pin-out of the (Reference) Pressure Sensor Case Connector

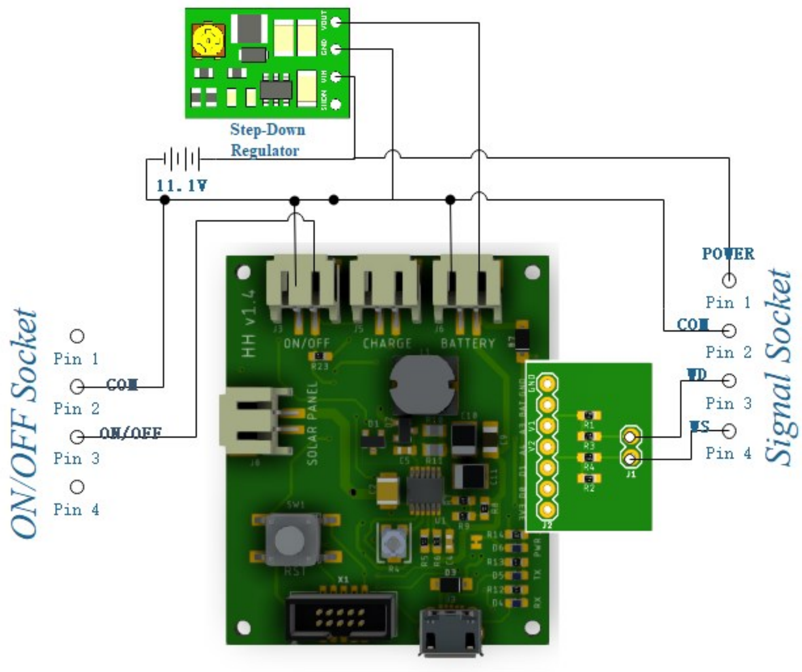

Figure 47 Pin-out of the Anemometer Box Connector

The pressure and anemometer measurements were calibrated during the development of the system, which is the key to reading the accurate data. For pressure calibration, a JOFRA compact pressure calibrator (CPC) pumps air to the pressure sensor and records the actual differential data, which will be compared to the digital values of the pressure sensor recorded in the WSN system (Figure 48). Wind speed and direction are calibrated with Panther 1000 Wind tunnel from FIT. The pitot tube of the wind tunnel collects the wind speed and compares the digital reading of the wind speed by the anemometer, which is placed into the testing chamber of the wind tunnel. The output of the wind direction is linearly related to the angle. It is straightforward to derive the transfer function of wind direction by slightly rotating the tail and reading the digital value near the degree of 0°. Record the maximum and minimum digital value on the FIT Hurricane House Monitor file, which corresponds to 359° and 0°, respectively. As the result of pressure and wind speed, the transfer functions are shown in Figure 50 and Figure 51. The wind direction calibration result is $y = 0.013x$

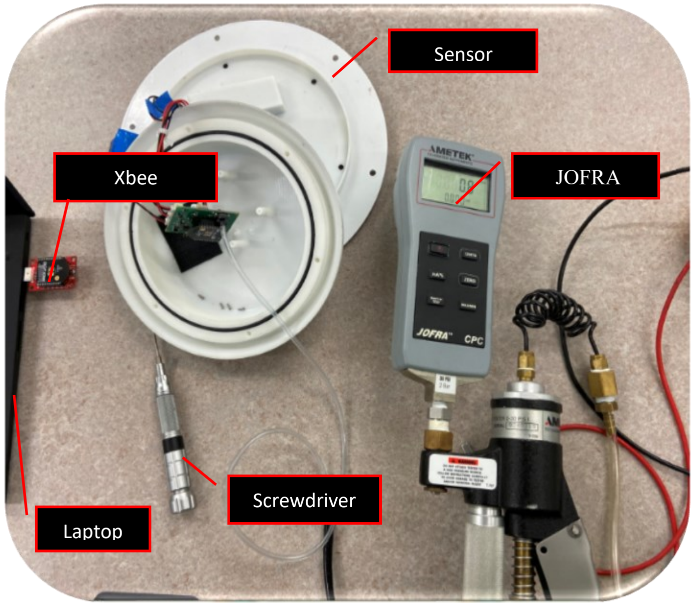

Figure 48 Instruments for Pressure Calibration

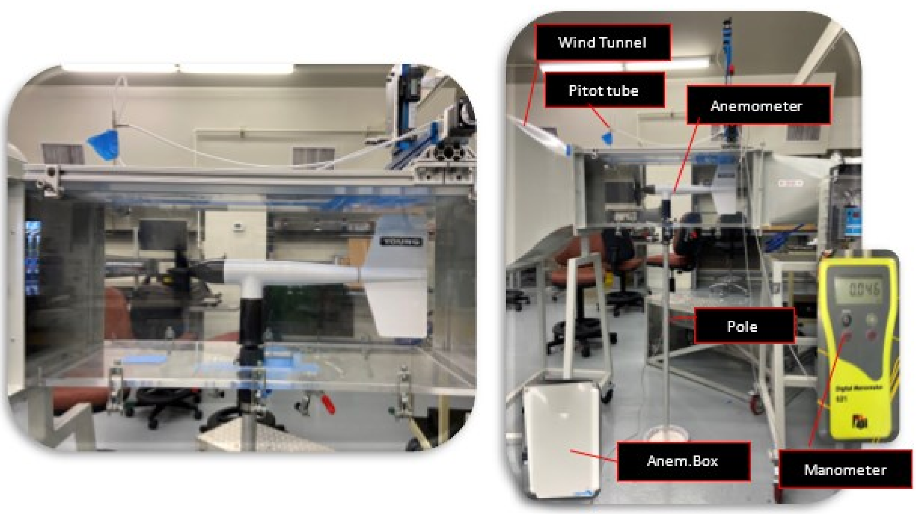

Figure 49 Instruments for Wind Speed and Direction Calibration.

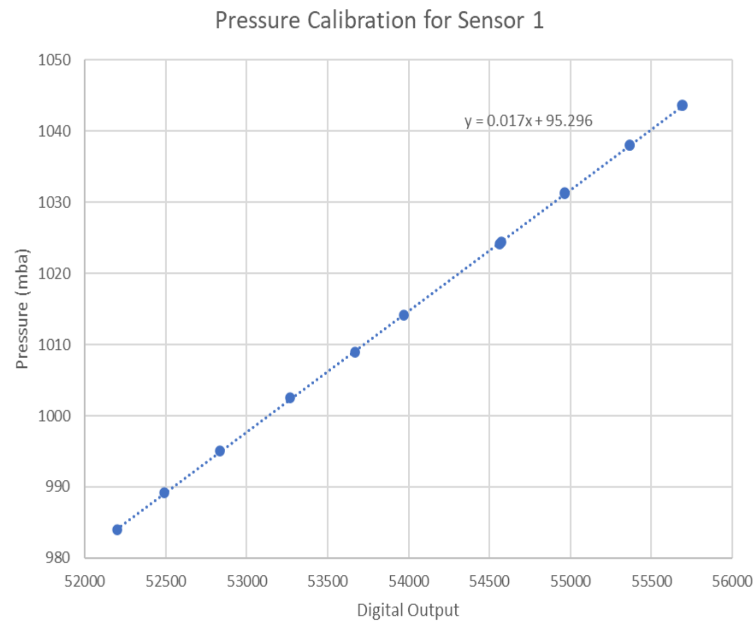

Figure 50 Pressure Calibration Result.

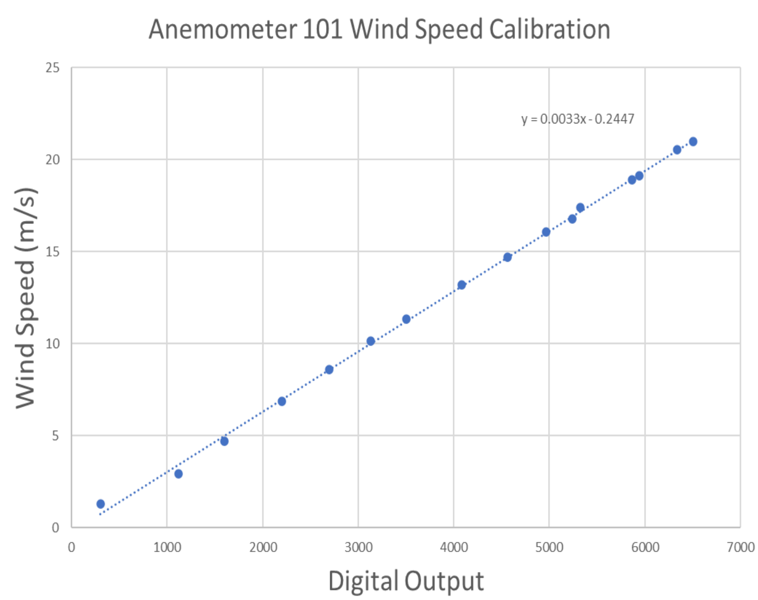

Figure 51 Wind Speed Calibration Result.